ANL/PPRNT--89-129

DE89 008388

A Simple Real Space Density Functional Theory of Freezing, with Implications for the Glass Transition

James Peter Stoessel*

Materials Science Division
Argonne National Laboratory, Argonne, IL 60439
and
School of Chemical Sciences
University of Illinois, Urbana, IL 61801

and

Peter G. Wolynes

School of Chemical Sciences
University of Illinois, Urbana, IL 61801

---

*Work supported by the U.S. Department of Energy, Basic Energy Sciences-Materials Science, under Contract W-31-109-ENG-38.

Manuscript submitted to J. Chem. Phys.

A Simple Real Space Density Functional Theory of Freezing, with Implications for the Glass Transition

James Peter Stoessel*

Materials Science Division
Argonne National Laboratory, Argonne, IL 60439
and
School of Chemical Sciences
University of Illinois, Urbana, IL 61801

and

Peter G. Wolynes

School of Chemical Sciences
University of Illinois, Urbana, IL 61801

Abstract

With analogy to the "highly accurate" summation of cluster diagrams for hard sphere fluids a la Carnahan-Starling, we present a simple, real space free energy density functional for arbitrary potential systems, based on the generalization of the second virial coefficient to inhomogeneous systems which, when applied to hard sphere, soft-sphere, and Lennard-Jones freezing, yield melting characteristics in remarkable agreement with experiment. Implications for the liquid-glass transition in all three potential systems are also presented.

---

*Work supported by the U.S. Department of Energy, Basic Energy Sciences-Materials Science, under Contract W-31-109-ENG-38.

I. Introduction

The study of phase transitions from a molecular viewpoint in physical systems is one of the most challenging problems in condensed matter physics. Although many workers in the field have developed numerous theories for the liquid-crystalline solid transition in model systems, questions concerning these theories still remain, in spite of the qualitative agreement with observation.[1-3] The theoretical situation is worse for the liquid-aperiodic solid transition. The lack of long-range order in these glassy systems precludes the use of well-established crystal physics techniques, and requires the application of new techniques to the solid phase. In addition, the actual nature and existence of the liquid-glass transition is unknown. The description of phase transitions is difficult because phases with different symmetries and structures require description within a single mathematical framework.

It has become popular recently to approach the problem of phase transitions from the viewpoint of liquid state physics. An early example of this is the work of Onsager concerning the effect of particle shape on the properties of colloids.[4] In it, he examines the isotropic-nematic liquid crystal phase transition using the general method of Mayer and Mayer to evaluate the free energy of the system in terms of the second virial coefficient generalized from the uniform fluid to include orientation by the introduction of an angle-dependent distribution function. Unable to evaluate higher order virial coefficients, Onsager approximates the third virial coefficient in terms of the second and ends the expansion at third order. This was inspired by Boltzmann's

evaluation of the third virial coefficient for hard spheres of equal diameter, in which he derives the relation between the two and three body cluster integrals.

Slightly earlier, Kirkwood and Monroe[5] developed a theory of freezing which was to become the precursor of modern density functional theories. In it they use the idea of variable coupling of one particle to the remaining N-1 particles to develop an integral equation relating $\rho(\vec{R})$, the single-particle density, to the liquid pair correlation function and the interparticle pair potential. Although this theory represented a major advance over existing "freezing" theories, the dependence of $\rho(\vec{R})$ on the pair potential prohibited the explanation of universal features during freezing.

Several events motivated the resurgence of the density functional theory of Kirkwood and Monroe, albeit in a slightly more general form. The unexpected observation of hard sphere solidification during the computer experiments of Alder and Wainwright[6] attracted much theoretical attention vis a vis hard sphere freezing. The possibility of using the liquid state as a reference state from which theoreticians could study HS freezing was realized by Wertheim's solution of the Percus-Yevick integral equation for the direct correlation function of hard spheres,[7] a fundamental advance in liquid state physics. The use of the hard sphere fluid as a reference state for more realistic systems was justified initially by the classic work of Longuet-Higgins and Widom,[8] in which they examined the effect of an attractive interaction on the melting properties of argon using the augmented van der Waals theory. Their work indicated the predominant role of repulsive forces in determining structures and coexistence parameters at melting.

In addition, Verlet's[9] study of the structure factor of classical fluids at melting, resulting in the empirical Verlet rule (analogous to the solid state Lindemann law), showed the "universality" of melting behavior vis a vis the structure factor, and also the legitimacy of the hard sphere model for systems with compliant potentials. The relation between the structure factor and the direct correlation function[10] directed workers, starting with Ramakrishnan and Yussouff,[11] to reconsider the Kirkwood-Monroe approach to freezing, with emphasis on free energy perturbation expansions of the solid about the uniform fluid, with the direct correlation function, now available, as the expansion coefficients. These are the "modern" density functional theories applied rather widely to a variety of phenomena: the liquid-solid interface,[12] liquid crystals,[13,14] nucleation,[15] glasses,[1] and freezing.[6,16]

In general, for the freezing problem there are two common features present in these density functional theories. First, one approximates the solid phase direct correlation function by that of the fluid, given by Wertheim.[7] This seems empirically reasonable in light of Verlet's melting rule. Thus, these density functional theories are better able to explain "universal" melting properties, in contrast to Kirkwood-Monroe theory. Secondly, the periodic density distribution of the solid is written as a Fourier series in the reciprocal space of the nonuniform phase.

Although these approaches have met with success, there have been recent questions concerning the nature of that success. Baus and Colot[2] and Jones and Mohanty[19] have recently addressed the use of a reciprocal space description for the hard sphere solid. They find that $\rho(\vec{r})$, the single particle density, when written in reciprocal space, as is done in

most density functional theories,[44] shows regions of negative values, clearly unphysical. This behavior results from the truncation of the Fourier expansion after two terms, rendering questionable the description of sharp features in $\rho(\overline{r})$ in the high density solid. They further suggest that the good agreement seen with these theories is a consequence of cancellation of errors, i.e., errors in approximating the solid direct correlation function by the fluid direct correlation function cancels the errors introduced via a reciprocal space description of $\rho(\overline{r})$. Others (12,16) use the reciprocal space description of the solid in a more appropriate way, with no regions of negative density. This approach is fine for the liquid-crystalline solid transition, where one has knowledge of the reciprocal lattice, and summation over twenty or so reciprocal lattice vectors is possible. For a description of vitrification, however, summation over the reciprocal lattice would correspond to twenty or so variational parameters (45). This is clearly unpalatable.

Concerns about the use of fluid phase direct correlation functions to describe solid-phase correlation and the sensitivity of transition parameters to the direct correlation function have also recently been addressed. Singh, et.al.[1] presented a real-space density functional description of the hard-sphere glass, based on the uniform fluid direct correlation function, c(r). They found extreme sensitivity of liquid-glass transition behavior to the form and values of the high density c(r) used. Haymet[3] finds the unphysical feature of "remelting" in the high density hard sphere fcc crystal, and attributes this to the inadequacy of the liquid structure factor at these densities. Baus and Colot go beyond questioning the <u>form</u> of the fluid c(r), and question the <u>use</u>

of the liquid c(r) to describe the solid phase. They indicate that the usual procedure of expansion of the solid c(r) about the fluid c(r), and truncation at second order, neglects density variations of c(r) in the critical region and thus presumably leads to incomplete convergence of the functional expansion. These are the major problems associated with the usual density functional descriptions of freezing. There have been attempts to circumvent these difficulties.

The real space description of $\rho(\vec{r})$, introduced by Tarazona,[17] has been used by Singh et.al.[1] in the glass transition problem, and by Baus and Colot,[2] Mohanty and Jones,[19] and Tarazona,[20] in their analysis of hard sphere freezing. In this description, $\rho(\vec{r})$ is approximated as a sum of Gaussian peaks, each centered at a lattice site of the nonuniform solid. Experimentally, the Gaussian solid is appropriate,[21,22] and this form of $\rho(\vec{r})$ has eliminated the problems associated with the description of sharp features in the density distribution of solids. For the glass transition problem, the switch from reciprocal to real space corresponds to a reduction in the number of variational parameters (45). Baus and Colot[18] observe <u>no</u> remelting at high solid densities, up to close packing, when using the Gaussian solid. On this last point, there are questions. It is not clear that the different prescription for solid phase correlations used by the authors is not a contributing factor to appropriate high density behavior. Regardless, the transition parameters obtained for hard sphere freezing, when employing the Gaussian solid, are in very good agreement with experimental results, despite the use of

various forms of c(r). It seems unquestionable that a real space $\rho(\vec{r})$ offers an efficacious alternative to the reciprocal space description so often seen.

We now turn to the problem of solid phase correlations in density functional theories. There are two notable attempts to deal with this question. Baus and Colot[2] have approximated the direct correlation function of the solid by an effective liquid direct correlation function, since one has information about this object from liquid state theory. The effective liquid scales with the solid, i.e., the smallest reciprocal lattice vector of the solid is forced to coincide with the position of the main peak in the effective liquid structure factor. One finds the average density of the liquid which satisfies this scaling. Good results have been reported with this theory, especially at high density (viz. no remelting). Tarazona[17,20] has chosen to avoid the difficulties with high density liquid c(r) values by presenting a density functional theory in which he uses a local free energy functional, appropriate for slowly varying density waves, and justifies its functional dependence on the rapidly varying $\rho(\vec{r})$ by course-graining $\rho(\vec{r})$ over a region of configuration space given by an unspecified weight function. The weight function is then determined by requiring self-consistency between the Percus-Yevick direct correlation function and Tarazona's derived c(r). The derived structure factor, at freezing, is in good agreement with the Hansen-Verlet rule, and coexistence densities are well reproduced. High density behavior has not been addressed.

In our pursuit of a density functional description of the liquid-aperiodic solid phase transition, and of the thermodynamic properties of the high density solid, we were led to a realization of the problems

associated with solid correlation functions and density wave descriptions.[1] In the course of trying to deal with these difficulties, we have developed what we believe to be the simplest real space density functional theory of hard sphere freezing, with the most promise for extension to the case of arbitrary potentials. Coexistence parameters are very faithfully reproduced, and the high density solid pressures are in remarkable agreement with the exact compressibilities given by Salsburg and Wood,[23] both for crystalline and amorphous packings.

Later we will see that for smoothly varying density distributions, free energy values from this functional are expected to be quite accurate for low to moderate mean densities. For moderately nonuniform particle distributions, there is uncertainty in our approximate density functional. However, the remarkable pressure agreement alluded to above, and shown later in Section III, allows us to have confidence in the relations we assume between lower and higher order virial coefficients for the high density, nonuniform system as well as to speculate as to the nature of the liquid-glass transition.

In retrospect, our present theory is very reminiscent of Onsager's theory of the isotropic-nematic liquid crystal system mentioned earlier. Our theory, at the lowest level, resembles Onsager's if one associates his orientational distribution function with our single particle density, $\rho(\vec{r})$.

In Section II, we present the motivation and derivation of the free energy functional. In Section III, we consider hard sphere freezing, and implications for the hard sphere glass transition. Section IV treats freezing and vitrification for the inverse-12 and Lennard-Jones potentials. We conclude our discussion in Section V.

II. Theory

We begin by considering N spherical atoms in a uniform fluid, of volume V and temperature T, with mean density ρ_o, interacting via a pair potential $\phi(r)$. When analyzing the uniform fluid-nonuniform solid phase transitions, one must develop an expression for the free energy which reflects particle distributions appropriate to the stable equilibrium phase. For example, when a liquid freezes into a crystal, there is a discontinuous change in the single particle distribution, from one which is uniform and translationally invariant to one which is nonuniform with broken translational symmetry. An appropriate free energy functional would exhibit a minimum for a uniform distribution of particles at liquid densities, but for mean densities in excess of the melting density, the minimum free energy should be obtained with a spatially varying density characteristic of the crystal.

To accomplish this analysis, one requires a trial function capable of describing the single particle distribution in both uniform and nonuniform phases, along with an expression for the free energy, considered to be a functional of this local density.

IIA. Free Energy Functional

The following summary follows the work of Yang, Fleming, and Gibbs.[24] We assume the existence of a single particle distribution function, $\rho(\overline{r})$, which describes the local density of particles at point $\overline{r}$, and leave until later the explicit specification of $\rho(\overline{r})$. We are therefore considering a nonuniform system.

The total configurational energy of the system is:

$$V(\bar{r}^N) = \sum_{i<j}^{N} \phi(|\bar{r}_i - \bar{r}_j|) + \sum_{i=1}^{N} U(\bar{r}_i) \qquad \text{(II.A.1)}$$

here $\bar{r}_i$ denotes the position of the i^{th} atom, $\bar{r}^N$ is equivalent to $\bar{r}_1$, $\bar{r}_2$, ..., $\bar{r}_N$, and $U(\bar{r}_i)$ represents some arbitrary external single particle potential which couples with the density at $\bar{r}_i$. We will work in the rand canonical ensemble, within which particle number fluctuations are asily treated. This is the natural choice for theories of phase transitions.

Given $V(\bar{r}^N)$, the configurational grand potential, W, is given by:

$$Z(V,T) = e^{W} = \sum_{N=0}^{\infty} \frac{1}{N!} \int \prod_{i=1}^{N} d\bar{x}_i \prod_{i<j} \{1+f(\bar{x}_i,\bar{x}_j)\} \prod_{i=1}^{N} e^{\xi(\bar{x}_i)} \qquad \text{(II.A.2)}$$

here

$$f(\bar{x}_i,\bar{x}_j) = \exp[-\beta\phi(\bar{x}_i,\bar{x}_j)]-1$$

$$\xi(\bar{x}_i) = \beta\mu - \beta U(\bar{x}_i)$$

$$\beta = (k_B T)^{-1}$$

nd μ is the chemical potential. We have set Λ, the thermal deBroglie avelength to unity in II.A.2, since this introduces the same constant ontribution to the free energy of both phases, and can thus be ignored, thout loss of generality. We can imagine probing the system with our ternal field, $U(\bar{x})$, and obtaining information about the single partie distribution, $\rho(\bar{x})$. The relation between field and density is obined with the realization that W, from II.A.2, is a functional of

$\xi(\bar{x})$, the effective single particle potential, and, of course, the pair interaction, $\phi(\bar{x}_i,\bar{x}_j)$. We concern ourselves only with single particle properties at the moment. Functional differentation of W with respect to $\xi(\bar{x})$ yields, from II.A.2, the following relation:

$$\frac{\delta W}{\delta \xi(\bar{x})} = \langle \rho_M(\bar{x}) \rangle \equiv \rho(\bar{x}) \qquad \text{(II.A.3)}$$

where

$$\rho_M(\bar{x}) = \sum_{i=1}^{N} \delta(\bar{x}-\bar{x}_i) \quad .$$

We will see that II.A.3 gives a trivial relation between field and density for the ideal gas. To examine thermodynamic properties of the bulk phases, we make contact with the Helmholtz free energy:

$$\begin{aligned} \beta F &= \beta\mu N - \beta PV = \beta\mu N - W \\ &= \int d\bar{x}\rho(\bar{x})\xi(\bar{x}) + \int d\bar{x}\rho(\bar{x})U(\bar{x}) - W \qquad \text{(II.A.4)} \\ &= F' + \int d\bar{x}\rho(\bar{x})U(\bar{x}) \end{aligned}$$

where

$$F' = \int d\bar{x}\rho(\bar{x})\xi(\bar{x}) - W$$

In II.A.4, we have used the definition of $\xi(\bar{x})$ and the relation $\beta PV = W$. The definition of F' in II.A.4 is actually the Legendre transform of W, from the natural variable $\xi(\bar{x})$ to the variable $\rho(\bar{x})$. In fact, functional differentiation of F' with respect to $\rho(\bar{x})$ yields

$$\begin{aligned} \frac{\delta F'}{\delta \rho(\bar{x})} &= \xi(\bar{x}) + \int d\bar{x}'\rho(\bar{x}') \frac{\delta \xi(\bar{x}')}{\delta \rho(\bar{x})} - \int d\bar{x}'' \frac{\delta W}{\delta \xi(\bar{x}'')} \frac{\delta \xi(\bar{x}'')}{\delta \rho(\bar{x})} \\ &= \xi(\bar{x}) \end{aligned} \qquad \text{(II.A.5)}$$

using II.A.3.

Our goal, then, is to express $\xi(\bar{x})$ in terms of $\rho(\bar{x})$. We would then possess a free energy, via functional integration, which is a functional of our single particle distribution function. These are the relations we seek.

II.B. Ideal Gas Free Energy Functional

For a system with no internal interactions, $\phi(\bar{x}_i,\bar{x}_j) = 0$, and II.A.2 becomes

$$Z^{(id)}(V,T) = e^{W^{(id)}} = \sum_{N=0} \frac{1}{N!} \int \prod_{i=1}^{N} d\bar{x}_i e^{\xi(\bar{x}_i)} \qquad \text{(II.B.1)}$$

where "id" indicates the ideal gas condition. If the external field, $U(\bar{x})$, did not exist, II.B.1 would be the usual ideal gas partition function of uniform fluids. Using II.B.1 and II.A.3, we have:

$$\rho(\bar{x}) = \frac{\delta W^{(id)}}{\delta \xi(\bar{x})} = e^{\xi(\bar{x})} \qquad \text{(II.B.2)}$$

where we have used the fact that the grand potential is a natural function of volume, temperature, and chemical potential. From II.B.2, a trivial relation exists between the field and the density for the ideal gas. Substituting $\xi(\bar{x})$ from II.B.2 into II.A.5, and functionally integrating, we obtain the following expression for the ideal gas free energy:

$$\beta F_o' = \int d\bar{x}\, \rho(\bar{x})\{\ln[\rho(\bar{x})] - 1\} \qquad \text{(II.B.3)}$$

In the absence of all external fields, we see using II.A.4, that II.B.3 becomes our density functional expression for the ideal gas Helmholtz free energy for the nonuniform system.

II.C. Interaction Free Energy Functional

In II.B, we considered the system in the absence of pair interactions. We now turn on these interactions, and seek the interaction Helmholtz free energy as a single particle density functional.

The usual way to proceed is to functionally Taylor expand the interaction Helmholtz free energy of the nonuniform system about the uniform system. The details may be obtained elsewhere.[24] The basic point is that the direct correlation function for the uniform phase acts like the expansion coefficient. The object is not known, and so one approximates the direct correlation function of the uniform phase. In Section I, we examined some of the problems associated with this approximation.

In a different spirit, we propose to consider explicitly the virial expansion of the nonuniform solid, graphically represented as:

$\beta PV =$ 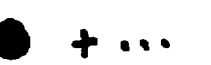 $+ \cdots$ (II.C.1)

where field points are weighted by the single particle density, $\rho(\overline{x})$, and are connected by Mayer f-bonds of II.A.2. This is a generalization of the uniform fluid equation of state, where field points are weighted by the mean, uniform density, ρ_o. The complete graphical theory of this expansion is contained in the classic work of Morita and Hiroike.[25]

In general, the full series in II.C.1 cannot be evaluated. For clusters with three or more atoms, the fiducial site structure is not always available. Even if these structures were at hand, the integrations implied by the cluster diagrams in II.C.1 are prohibitive, given the form for $\rho(\bar{x})$ which we have used in our theory. (Our choice of $\rho(\bar{x})$ will be discussed later.) We are thus left with a virial for which only the first term is readily available. We can take these higher order terms into account by generalizing the approach of Carnahan and Starling[26] to the nonuniform system. For continuity, we now review the Carnahan-Starling equation of state for the uniform hard sphere fluid.

For a uniform fluid, $\rho(\bar{x}) = \rho_o$, and differentiation of II.C.1 gives:

$$\frac{\beta P}{\rho_o} = \sum_{i=0}^{\infty} B_{i+1}(\rho_o)^i \qquad \text{(II.C.2)}$$

where

$$B_1 \equiv 1$$

$$B_2 = -\frac{1}{2} \int d\bar{x} f(x)$$

$$B_3 = -\frac{1}{3} \int d\bar{x} d\bar{x}' f(\bar{x},\bar{x}') f(\bar{x}) f(\bar{x}')$$

These integrals, of course, are the first few cluster diagrams of the uniform fluid virial series. As the order of the diagram increases, the difficulty in computation increases. Hence, only the lowest order terms in the virial series can be computed. For hard spheres, the first seven virial coefficients have been computed. B_2, B_3, and B_4 are analytically

evaluated (B_4 by Boltzmann!). The remaining three have been computed by Hoover and Ree[27] using the Monte Carlo technique. The results are expressed in the following seven term virial series:

$$\frac{\beta P}{\rho} = 1 + 4\eta + 10\eta^2 + 18.365\eta^3 + 28.24\eta^4 + 39.5\eta^5 + 56.5\eta^6 + \ldots$$

$$= 1 + \sum_{n=1}^{\infty} C_n(\eta)^n \qquad \text{(II.C.3)}$$

where $\eta = \pi\rho\sigma^3/6$.

Carnahan and Starling replaced C_3 with the closest integer (i.e. $C_3 = 18$) and assumed the following form for C_n:

$$C_n = a_1 n^2 + a_2 n + a_3 \qquad \text{(II.C.4)}$$

Solution of II.C.4 yields the following expressing for C_n:

$$C_n = n^2 + 3n \; . \qquad \text{(II.C.5)}$$

Using II.C.5 in II.C.3, Carnahan and Starling obtained the following heuristic equation of state:

$$\frac{\beta P}{\rho} = 1 + \sum_{n=1}^{\infty} (n^2 + 3n)(\eta)^n \qquad \text{(II.C.6)}$$

Expressing II.C.6 as a linear combination of the first and second derivatives of the geometric series, $\sum_{n=1}^{\infty} (\eta)^n$, they obtained the famous Carnahan-Starling equation of state:

$$\frac{\beta P}{\rho} = \frac{1+\eta+\eta^2-\eta^3}{(1-\eta)^3} \qquad \text{(II.C.7)}$$

Equation II.C.7 agrees remarkably well with computer simulation results over the entire fluid density range.

From standard thermodynamic identities,[10], the interaction Helmholtz free energy for the hard sphere fluid may be obtained in closed form, using II.C.7:

$$\frac{\beta F^{(int)}}{N} = \int_0^{\eta} \frac{d\eta'}{\eta'}\left[\frac{\beta P}{\rho'} - 1\right]$$

$$= \frac{\eta[4-3\eta]}{[1-\eta]^2} \qquad \text{(II.C.8)}$$

Our semiempirical interaction free energy functional derives from the assumption that for the nonuniform system, the relation of higher to lower order virial coefficients has the <u>form</u> of the Carnahan-Starling virial series. Thus, comparing II.C.3, and II.C.1, we arrive at the following identification:

$$\eta[\rho(\bar{x})] = -\frac{1}{8N}\int d\bar{x}d\bar{x}'\ \rho(\bar{x})\rho(\bar{x}')f(\bar{x},\bar{x}') \qquad \text{(II.C.9)}$$

Equation II.C.9 represents a <u>generalized packing fraction</u> or <u>generalized second virial coefficient</u> which is a function of the interparticle potential and the structure of the nonuniform phase. In terms of $\eta[\rho(\bar{x})]$, the interaction Helmholtz free energy for the nonuniform system is:

$$\frac{\beta F^{(int)}}{N} = \frac{\eta[\rho(\bar{x})]\{4-3\eta[\rho(\bar{x})]\}}{[\,1-\eta[\rho(\bar{x})]\,]^2} \qquad \text{(II.C.10)}$$

If we were to consider ellipsoidal particles, $f(\bar{x},\bar{x}')$ in II.C.9 would be orientational dependent. Replacing $\rho(\bar{x})$ with an orientational distribution function, and linearizing II.C.10, one obtains basically the Onsager expression for the interaction free energy of liquid crystals. Rather than stop at third order, as Onsager did, we have presumably

incorporated higher order free energy clusters via the form of II.C.7 and II.C.10. Equation II.C.10, combined with II.B.3, furnishes us with a density functional expression for the Helmholtz free energy of the nonuniform system. To proceed, one requires an expression for the single particle distribution, $\rho(\overline{x})$. We now consider this.

II.D. The Local Density

In order to apply our free energy functional, we need an expression for the local density, $\rho(\overline{x})$. In most previous treatments of freezing involving density functional theory, the periodicity of the solid lattice is incorporated in $\rho(\overline{x})$ by Fourier expansion into plane waves. This yields the well-known density wave or order parameter expansion. Typically, then, this expansion is truncated for numerical tractability. This approach, however, if applied to disordered solids, has difficulties, as discussed in Section I.

Previously,[1] we used the real space description of $\rho(\overline{x})$ suggested by Tarazona.[17] We adopt this description in our present theory. Accordingly, we write $\rho(\overline{x})$ as an expansion of Gaussian density peaks centered at each fiducial site in the nonuniform system:

$$\rho(\overline{x}) = \left(\frac{\alpha}{\pi}\right)^{3/2} \sum_{\overline{R}} e^{-\alpha(\overline{R}-\overline{x})^2} \qquad \text{(II.D.1)}$$

In II.D.1, $\{\overline{R}\}$ is the set of fiducial site positions, $\{\overline{x}\}$ the set of particle positions, and α measures the peak width. The normalization ensures that the integrated density peak is unity, so that the lattice constant is fixed by the mean density. Computer simulation results[21,22]

indicate that a harmonic description of particle displacements, seen in II.D.1, is appropriate, even at melting. The periodicity of the lattice is incorporated via the sum over lattice vectors.

For the high densities considered in freezing theories, the width of these Gaussian peaks is very small (i.e., particle displacements are small), making overlap negligible. Thus, the expansion II.D.1 converges more rapidly than reciprocal space expansions. The rapid convergence of II.D.1 was demonstrated previously,[1] with regard to the large-α approximation for the ideal gas free energy, equation II.B.3. There, it was found that, for $\alpha \geq 5$, the approximated ideal free energy (with only nearest-neighbor overlap taken into account in $\rho(\overline{x})$) and the "exact" ideal free energy (with the full $\rho(\overline{x})$ expansion) were essentially identical.

In the large α limit, particle excursions from fiducial sites are small, and as α approaches infinity, the particles localize at the fiducial sites. It is clear that

$$\lim_{\alpha \to \infty} \rho(\overline{x}) = \sum_{R} \delta(\overline{x}-\overline{R}) \qquad \text{(II.D.2)}$$

which can be recognized as the single particle distribution of a low temperature, high density classical solid.

In the opposite α limit, particle excursions are infinite, and the single particle distribution becomes uniform by adding flat, overlapping Gaussian density peaks, i.e.,

$$\lim_{\alpha \to 0} \rho(\overline{x}) = \rho_o \qquad \text{(II.D.3)}$$

This limit may be considered a description of the uniform fluid.

Given a set of fiducial sites, {R}, one now has a local density description in terms of a single parameter, α.

II.E. Large and Small α Behavior

Substitution of II.D.1 into II.B.3 and II.C.10, using II.C.9, gives an α-dependent Helmholtz free energy.

We now examine the large and small α limits to this free energy, starting with the ideal gas term, equation II.B.3. As discussed previously[1] substitution of II.D.1 into II.B.3 yields numerically complicated expressions for the ideal gas free energy for general α. To proceed, approximate expressions, for small and large α, can and have been developed which yield easily to computation. For completeness, Appendix I reviews the large and small α limits. The upshot of this analysis is that, for small α, the uniform fluid is the appropriate limit, as in II.D. 3, and II.B.3 reduces to the well-known ideal gas free energy of a uniform fluid

$$\lim_{\alpha \to 0} \frac{\beta F_o'}{N} = \ln(\rho_o) - \frac{3}{2} \qquad \text{(II.E.1)}$$

In the opposite limit we obtain

$$\lim_{\alpha \to \infty} \frac{\beta F_o'}{N} = \frac{3}{2} \ln\left(\frac{\alpha}{\pi}\right) - \frac{5}{2} \qquad \text{(II.E.2)}$$

The consideration of both limiting expressions shows that the ideal gas free energy is a monotonically increasing function of α. This behavior is expected. The small α fluid phase is one of maximum entropy.

We consider now the small α limit of the interaction free energy, equation II.C.10. In this limit $\rho(\vec{x}) = \rho_o$, and we have

$$\lim_{\alpha \to 0} \eta(\alpha) = -\frac{\rho_o}{8} \int d\vec{x} f(x) \qquad \text{(II.E.3)}$$

For the hard sphere potential, the integration leads to the usual packing fraction as the appropriate limit. For a general repulsive potential, one obtains an effective packing fraction.

In liquid state perturbation theory, the repulsive potential would be replaced by a hard sphere potential, with an effective hard sphere diameter, and thus, an effective packing fraction. In our theory, there is no need to invoke the idea of an effective hard sphere diameter. Equation II.E.3 incorporates the effects of potential energy compliance on the packing fraction.

In this limit, II.C.10 becomes the Carnahan-Starling interaction free energy, employed so successfully in the theory of uniform fluids.

In the opposite limit, substitution of II.D.1 into II.C.9 gives

$$\lim_{\alpha \to \infty} \eta(\alpha) = \frac{1}{8} + \text{constant} \qquad \text{(II.E.4)}$$

In Appendix III, we see what this constant is.

For an arbitrary repulsive potential, the value of $\eta(\alpha)$ obtained depends on two length scales: the range of the pair potential and the nearest-neighbor fiducial site separation.

II.F. The Variational Procedure

At this point, we possess the ideal gas and interaction free energies as functions of α. Variation of α from zero to infinity corresponds to the structural transition from the uniform fluid to the nonuniform phase [cf. Eqn. II.D.2-II.D.3]. By evaluating the total Helmholtz free energy as a function of α, we can determine the minimum free energy and the corresponding non-zero α value, and, thus, the equilibrium structure, of the solid system.

Characteristically, we observe no finite α free energy minimum for densities below a critical value ρ_c. The system is uniform fluid. For $\rho \geq \rho_c$, a finite α minimum appears. We therefore have a nonuniform equilibrium system, whose structure is described by II.D.1, a spatially varying density distribution. Comparison of uniform fluid (α=0) and nonuniform solid free energies determines which state is thermodynamically stable, and which is metastable.

For comparison with the fluid, we use the zero α limit to evaluate the fluid free energy. We specify the fluid free energy in this way for the following reasons. If one evaluates the <u>total</u> free energy as a function of α, for <u>all</u> α, one needs to interpolate between the small-and

large-α forms of the ideal gas free energy, given by A.I.5 (or A.I.6), A.I.11, A.I.15 (or A.I.16). When we use a third degree polynomial interpolation, we obtain, for all relevant densities, a smooth ideal gas free energy, for $0 \leq \alpha \leq \infty$. However, the total free energy shows two non-zero α minima, α_1 and α_2 ($\alpha_1 < \alpha_2$), for $\rho < 1.3$. α_1 versus ρ is nonmonotonic, with a fractional free energy charge, relative to the α=0 free energy, of .03. We therefore choose the zero α free energy as our description of the fluid free energy, and regretfully report that an unconstrained free energy minimization will not yield the zero α free energy and structure for the fluid. For $\rho > 1.3$, the α_1 minimum disappears, and free energy minimization yields two minima, one at α=0, and one at α_2. The minimum at α_2 is physically reasonable, and serves as the basis for all solid phase results reported herein. In all cases considered, the α_1 value lies in the interpolation region. Thus, the slight minimum at α_1 (relative to the α=0 free energy) is possibly due to numerical error. The α_2 value always lies in the large-α region, where no uncertainty in free energy exists. We are thus confident of our α_2 values. The equilibrium coexistence parameters can be determined by equating the pressures and chemical potentials of both phases at the transition, viz,

$$\mu_u(\rho_u) = \mu_n(\rho_n)$$
$$P_u(\rho_u) = P_n(\rho_n) \qquad \text{(II.F.1)}$$

where

$$\mu \equiv \frac{\partial \hat{f}(\rho_o)}{\partial \rho_o}$$

$$P \equiv \mu\rho_o - \hat{f}(\rho_o)$$

$$\hat{f}(\rho_o) \equiv \rho_o f(\rho_o)$$

and $f(\rho_o)$ is the density dependent free energy per particle. In II.F.1, the subscripts "u" and "n" denote uniform and nonuniform phases, respectively. The free energy per particle, used in II.F.1 to evaluate chemical potential and pressure, is determined for the nonuniform fluid by the following equation:

$$\beta f(\rho_o) = \beta f(\alpha - \alpha_{min}) \qquad \text{(II.F.2)}$$

where α_{min} denotes the minimum free energy α value.

In summary, we now possess what we believe to be the simplest density functional expression for the Helmholtz free energy of an arbitrary repulsive potential system. The extension to arbitrary potentials (i.e. repulsive and attractive forces) will be presented in the application sections of this paper. Given any nonuniform system, knowledge of the zero temperature structure and pair interaction allows a trivial description of the single particle distribution and thermodynamics of both phases on the same mathematical footing. There is no need to invoke different theories to describe the uniform fluid and nonuniform solid. Coexistence parameters, in the case of phase transformation, may also be obtained easily. We now apply our density functional theory to specific systems, beginning with the hard sphere potential.

III. The Hard Sphere System

We consider first the problem of hard sphere (HS) freezing. In Section III.B, application to the HS aperiodic solid is presented.

III.A. Hard Sphere Freezing

In this case, the set of fiducial sites, $\{\vec{R}\}$, which characterizes the local density, $\rho(\vec{x})$, is given by the Bravais lattice vectors of the face-centered cubic lattice (fcc). This set incorporates the translational symmetry of the lattice. The only other requirement for the specification of lattice structure is the lattice constant, a, fixed by the mean density ρ_o:

$$\rho_o = \frac{4}{a^3} \qquad \text{(III.A.1)}$$

With this information, the single particle distribution is known. In order to proceed, the pair potential must be given. For the HS system, we have:

$$\phi(r) = \infty \ , \ r \leq \sigma_{HS}$$

$$\phi(r) = 0 \ , \ r > \sigma_{HS} \qquad \text{(III.A.2)}$$

where σ_{HS} is the hard sphere diameter. We are now able to evaluate expressions II.C.9, II.C.10, and II.B.3, i.e., the ideal and interaction Helmholtz free energy, as a function of a. For general a, II.C.9 is evaluated numerically. Appendix II presents Equation II.C.9 in ready-to-use form. For the calculation of II.B.3, the ideal gas free energy, it is found that for all potentials and structures studied

herein, use of II.E.2, the large-α formula, to approximate II.B.3 incurs an error of less than a per cent for all α values consistent with a mechanically stable nonuniform phase.

As an example of the variational procedure, we show, in Figure 1, the competition between the ideal gas and interaction free energies, the former minimum at $\alpha = 0$, the latter at $\alpha \to \infty$. It is the balance of entropic and energetic forces which generates the equilibrium state. Also shown is the α-dependent total free energy, $\beta f(\alpha)$. For the mean density considered ($\rho_o \sigma_{HS}^3 = 1.0$) a minimum exists at $\alpha = 71$. Therefore, this equilibrium state is nonuniform solid, whose free energy per particle, at this density, is $\beta f_n(\rho_o^* = 1.0) = 4.27$.

The uniform liquid free energy is given as the $\alpha \to 0$ limit of $\beta f(\alpha)$, according to II.E.1 and II.E.3. For this example, the uniform fluid free energy is $\beta f_u(\rho_o^* = 1.0) = 4.09$. Consequently, although fluid and solid are both predicted equilibrium states, the uniform fluid is the thermodynamically stable state.

By use of this variational method, at each density, we proceed to evaluate the density dependent free energy per particle for both uniform and nonuniform phases viz.

$$\beta f_u(\rho_o) = \beta f(\rho_o;\ \alpha = 0)$$

$$\beta f_n(\rho_o) = \beta f(\rho_o;\ \alpha_{min}) \qquad \text{(III.A.3)}$$

with α_{min} fixed by the $\alpha \neq 0$ minimum of $\beta f(\alpha)$. In Figure 2, we show the free energy density as a function of density, $\beta f(\rho_o)$, for both uniform liquid and nonuniform, fcc solid. Below $\rho_o = .92$, no finite α minimum

exists and thus the system is pure liquid. For $.92 < \rho_o < 1.025$, the crystal exists, though it is metastable. Above $\rho_o = 1.025$, the crystal is the stable equilibrium phase.

The coexistence densities for the liquid-crystalline solid phase transition, as well as the melting pressure, P_m, may be obtained via II.F.1. We have also calculated the entropy change upon freezing, given in general by

$$\frac{\Delta S}{Nk_B} = (k_B T)\frac{\partial \Delta w}{\partial (k_B T)} \qquad \text{(III.A.4)}$$

where Δw is the change in grand thermodynamic potential per particle,

$$\Delta w = A\left(\frac{\beta P}{\rho}\right) \qquad \text{(III.A.5)}$$

In addition, we have evaluated the Lindemann ratio,[28] defined as:

$$\theta = \frac{[\langle \bar{x}^2 \rangle]^{1/2}}{d} = \frac{1}{d(2\alpha)^{1/2}} \qquad \text{(III.A.6)}$$

where $\bar{x}$ is the particle displacement vector from the fiducial site, and d is the fiducial site nearest-neighbor distance, which, for the fcc crystal, is given by

$$d = \frac{(2)^{1/6}}{(\rho_o)^{1/3}} \qquad \text{(III.A.7)}$$

These quantities are all shown in Table I, along with results from computer simulation and other freezing theories.

In Table I, ρ_f and ρ_s are the fluid and solid coexistence densities, respectively, P_m is the melting pressure, and $\Delta S/Nk_B$ is the entropy change on freezing. The variables θ_i, θ_t, and θ_m are the

Lindemann ratios for the following three conditions, respectively: (1) The point of marginal mechanical stability of the solid, (2) the point of marginal thermodynamic stability relative to the fluid at the same density, i.e., fluid and solid free energies are equal, and (3) the point of phase coexistence.

The "experimental" results labeled by A in Table I are the Monte Carlo results of Hoover and Ree,[29] and also the molecular dynamics results of Young and Alder.[22]

In row C, we present the results of Jones and Molanty.[19] These authors use the real-space, Gaussian description of the solid, equation II.D.1, and the free energy density functional obtained via thermodynamic expansion about the uniform fluid. For solid phase correlations, they use the liquid state Percus-Yevick direct correlation function. Treating the Gaussian peak width and lattice constant as variational parameters, they minimize the Helmholtz free energy to obtain the results shown. They therefore allow for variation in the set of fiducial sites, $\{\vec{R}\}$, and thus are able to incorporate lattice inhomogeneities in their approach.

Notice that Tarazona obtains three sets of coexistence densities, labeled D, E, and F. The values shown in D were obtained by using a constant value for his weight function when course-graining $\rho(\vec{x})$, as explained in Section I. In E, he uses a linear form for the weighting. Row F presents his most recent results, obtained with a density dependent weighting function, written as a Taylor series in density. The expansion coefficients are determined via the self-consistency criterion alluded to in Section I.

The results of Baus and Colot are shown in row G. Their approach to hard sphere freezing has already been explained (Section I).

Haymet[16] has recently treated hard sphere freezing, using the reciprocal space description of the solid density wave. For his density functional, he uses the thermodynamic expansion of the free energy about the uniform fluid, with solid phase correlations approximated by the uniform liquid direct correlation function. With use of the Wertheim-Thiele solution to the Percus-Yevick approximation for fluids, he finds the coexistence parameters labeled by H.

Subsequently,[3] Haymet has used the more accurate Henderson-Grundke direct correlation function,[30] and finds improved results, shown by row I in Table I.

Notice, in table I, that <u>all</u> reported density functional theories predict θ_m values which are considerably lower than those obtained from computer simulation. A possible explanation for this is implicit in the work of Hoover and Ree (29). They suggest that solid phase pressure, near melting, may be underestimated in their calculations, due to unphysical cell constraints. This, if true, would certainly overestimate free volume and Lindemann ratios, since the authors approximate solid phase pressures via a free volume expansion.

By appropriate differentiation of the solid free energy density, we have obtained the pressure behavior of the hard sphere crystal and have plotted this in Figure 3. Also shown for comparison is the pressure obtained from free volume theory,[31] and known to be exact in the high density solid as close-packing is approached,[23] viz,

$$\frac{\beta P}{\rho} = \frac{3}{(1-\frac{\rho}{\rho_{cp}})} \qquad \text{(III.A.8)}$$

Clearly, the agreement in pressure is remarkable. Not only do we see this agreement numerically, but, as shown in Appendix III, we expect such behavior analytically in the high density limit.

Given the extreme accuracy in solid phase pressure, liquid phase free energy, and coexistence parameters, we can be assured of the appropriateness of the solid phase description offered by $\rho(\overline{x})$ in II.D.1.

In light of this presumably correct description for the hard sphere crystal, we show, in Figure 4, the density dependence of the equilibrium α value, written in terms of the Lindemann ratio, θ, given in III.A.6. At the solid coexistence density, $\alpha_{min} \approx 150$, which corresponds to density fluctuations occurring on a length scale of $\approx .053\ \sigma_{HS}$. As density increases, this length scale obviously diminishes. As discussed before, such short-ranged behavior necessitates the inclusion of very high order reciprocal lattice vectors in any reciprocal space density functional treatment of hard sphere freezing. This numerical restriction limits these theories to low solid densities. In view of the results obtained with our density functional theory, the description of the extremely high density crystal is within the capability of this new approach.

III.B. Aperiodic Hard Sphere Solid

It is perhaps not surprising that a density functional theory of hard sphere freezing with uniform, harmonic atomic displacements from known equilibrium sites works remarkably well for the high solid densities considered in the homogeneous environment of the fcc lattice. After all, the assumption of homogeneity and harmonicity of lattice displacements is the basis of all theories of lattice dynamics in the crystalline solid state.

The hallmark of the aperiodic solid state is, for our purposes, topological disorder. As one moves from one fiducial site to the next, the environment changes, and we therefore expect a distribution of averaged atomic displacements throughout the system. This is in contrast to the crystalline case, where all equilibrium sites have identical averaged environments. These site inhomogeneities present in the disordered solid bring into question the use of a one-parameter theory in the description of the solid state. The assumption of linearity is presumably still appropriate, as we are dealing with very small particle displacements at these high solid densities. Still, it is enlightening to begin any analysis with the simplest possible description, generating information which will further guide one to future considerations and refinements. It is for this reason that we consider now the present density functional theory applied to disordered lattices.

The aperiodic structure which we investigate is the set of fiducial sites given by Bennett using his computer packing algorithm.[32] The only other ingredient needed for the description of the nonuniform solid is the nearest-neighbor separation of fiducial sites, d_c, and this is determined by requiring that a system of hard sphere particles, with diameter d_c, be close-packed at the mean density ρ_o, i.e.

$$\eta_c = \frac{\pi}{6} \rho_o (d_c)^3 \qquad \text{(III.B.1)}$$

where η_c is the upper limit to the hard sphere packing fraction for the dense random packing of Bernal.[33] We use $\eta_c = .636$, although there is controversy as to what η_c actually equals.[34]

With $\rho(\overline{x})$ now prescribed, we evaluate the free energies of uniform fluid and disordered solid, as in Section III.A. Figure 2 shows the free energy density for the solid. Of course, the fluid free energy is already given in Figure 2, evaluated with the previously discussed crystal free energy.

Although an equilibrium solid phase exists, for $\rho_o > .97$, these solid states are metastable, relative to the uniform fluid. This behavior is in contrast to that observed for the same system, analyzed using a free energy expansion about the uniform fluid.[1] In that approach, using the Henderson-Grundke liquid direct correlation function, the Bennett lattice is found to be initially metastable, but for $\rho_o > 1.14$, the disordered solid becomes the stable phase, indicative of a first-order transition. As previously noted, however, this result is suggestive, and certainly, in light of the sensitivity of results to liquid state correlations, one must be cautious of the numerical results and implications. In fact, the authors note that, although they obtain liquid and solid free energy curve crossing, they are unable to determine transition parameters via a Maxwell construction, due to the negative pressures obtained for the liquid branch. They attribute the over estimate of solid stability to the ad hoc tail used in the direct correlation function.

In view of the accuracy with which hard sphere freezing parameters are obtained, the suggestion of metastability for the aperiodic solid throughout the entire solid density range, within the limitations of the present theory, appears to be on firmer ground than that given previously.

Further evidence that this present theory may faithfully describe the aperiodic solid is given by the pressure behavior obtained, and shown in Figure 3. The pressure of the disordered solid should be compared with that obtained from III.A.8 with ρ_{cp} =1.216. The derivation of III.A.8 is quite general, without regard to the exact close-packed structure, and requires only the value of the limiting close-packed density. The agreement seen between the"exact" pressure (i.e. III.A.8) and the calculated pressure of the Bennett lattice indicates that our density functional properly describes the shape of the solid free energy. Whether or not the free energy values are correct is not known. A real aperiodic solid contains deviations in fiducial site positions, as well as a distribution of Gaussian peak widths. It is conceivable that a free energy minimization in the disordered solid, treating the fiducial site positions and Gaussian peak widths in $\rho(\overline{x})$ as variational parameters, could yield a more realistic aperiodic solid structure and free energy values which admit a true thermodynamic transition, yet leaving the shape of the free energy curve unchanged.

This approach would be similar in spirit to the calculations of Jones and Mohanty[19], in their theory of hard sphere freezing. A difficulty which would be present in the aperiodic solid calculation, and is not present in the crystal calculation, is the specification of the initial fiducial structure, about which fiducial site deviations are incorporated in the variational procedure. Until such a calculation is complete, the aperiodic lattice is thermodynamically metastable, within the present theory.

In Figure 4, we show the density dependence of the Lindemann ratio for the aperiodic solid. It is interesting that, for both the fcc and Bennett structures, the Lindemann ratio is $\theta_i = .115$, suggesting that, regardless of structure, mechanical stability is destroyed *when* atomic displacements reach a certain fraction of the fiducial site separation.

We now examine the temperature dependence of coexistence parameters, as well as the effect of temperature on the thermodynamic properties of the fcc and Bennett solids, via the inverse-12 and Lennard-Jones potentials.

IV. Soft-Sphere Potentials

IV.A The Perturbation Calculation

In general, a soft-sphere potential differs from the hard sphere potential, equation III. A.2, in two ways: (1.) the repulsive force potential is not impulsive, but rather temperature dependent, allowing particle penetration to separations less than the particle diameter, and (2.) there exists a tail to the potential. The most popular way to treat such a potential, in liquid state theory, is to separate the full potential into a reference system and a perturbation, viz.

$$\phi(r) = \phi_r(r) + \phi_p(r) \qquad \text{(IV.A.1)}$$

The reference system, with strictly repulsive forces, is then replaced by an equivalent hard sphere system, with an effective temperature and density dependent hard sphere diameter. The perturbation potential is treated in perturbation theory, typically averaged over the pair correlation function of the fluid. It is the perturbation potential, then, which predominately determines the temperature dependence of coexistence parameters and bulk phase thermodynamic properties during freezing.

In this spirit, we treat the soft-sphere potential in the manner of Tarazona (17), i.e.

$$\beta f[\rho(\bar{x})] = \beta f_r[\rho(\bar{x})] + 1/2 \int d\bar{x}d\bar{x}' \, \rho(\bar{x})\rho(\bar{x}') \, \phi_p(|\bar{x}-\bar{x}'|) \qquad \text{(IV.A.2)}$$

where $\beta f[\rho(\bar{x})]$ is the total Helmholtz free energy per particle, $\beta f_r[\rho(\bar{x})]$ is the free energy of the repulsive potential reference system, and the last term in IV.A.2 treats the perturbation potential in

mean field fashion. Equation IV.A.2 is an augmented van der Waals theory, analogous to the theory of Longuet-Higgins and Widom discussed earlier, and also to the various perturbation theories of liquids.[10] Therefore, we expect IV.A.2 to be an adequate free energy approximation for weak and long-ranged perturbations, especially at the high densities which we are presently considering.

In IV.A.2, $\beta f_r[\rho(\bar{x})]$ is given by II.E.2, II.C.9, and II.C.10, using the actual repulsive reference potential, $\phi_r(r)$, in the specification of the Mayer f-bond. There is no need to reduce the reference system to an equivalent hard sphere system, as is done in liquid state perturbation theory. Although the mean field term in IV.A.2 treats particle correlations in the nonuniform phase implicitly, through the imposition of a lattice structure, particle correlations are not incorporated in the uniform fluid phase. At high temperatures, where the effect of the tail is negligible, this lack of correlation will not be a problem. At lower temperatures, though, it may be a drawback.

We now need to consider the question of how to separate the full potential into a reference system potential and a perturbation potential. To date, the most successful separation scheme and perturbation theory for classical equilibrium fluids is that of Kang, et al.[35] The method consists of dividing the potential into a reference potential and a perturbation potential at a break point, λ, which may depend on density. Mathematically,

$$\phi(r) = \phi_r(r) + \phi_p(r) \qquad \text{(IV.A.3)}$$

$$\phi_r(r) = \phi(r) - F(r) \quad \text{if } r \leq \lambda \qquad \text{(IV.A.4)}$$

$$\phi_r(r) = 0 \quad \text{if } r > \lambda$$

$$\phi_p(r) = F(r) \qquad \text{if } r \leq \lambda \qquad \text{(IV.A.5)}$$

$$\phi_p(r) = \phi(r) \qquad \text{if } r > \lambda$$

where λ and $F(r)$ are arbitrary. For λ, they use the following prescription:

$$\lambda = \text{Min}(d_{fcc}, r^*) \qquad \text{(IV.A.6)}$$

where r^* is the interparticle separation at the minimum of $\phi(r)$, and d_{fcc} is the nearest-neighbor separation in the fcc lattice, given by III.A.7. For $F(r)$, they use the following form:

$$F(r) = \phi(\lambda) - \phi'(\lambda)(\lambda - r) \qquad \text{(IV.A.7)}$$

where

$$\phi'(\lambda) = \left.\frac{d\phi(r)}{dr}\right|_{r=\lambda}.$$

The form chosen for $F(r)$ in equation IV.A.7 ensures the continuity of $\phi_r(r)$ and $\phi_p(r)$, as well as their derivatives, at $r=\lambda$.

The choice of λ is reasonable. At high densities, particle separations comparable to r^* are rare. Each atom is confined to a cage formed by the repulsive forces of its neighbors. Therefore, the equilibrium separation of the atoms will be roughly d_{fcc}. This choice of λ has the effect of reducing the range of $\phi_r(r)$ with increased density. This allows the calculation of equivalent hard-sphere diameters, for use in liquid state perturbation theory, which are physically reasonable and lead to excellent predictions of thermodynamic properties for classical fluids throughout the entire density and temperature range, when com-

bined with IV.A.7 and IV.A.3-5. Earlier separation schemes[36] have lead to overestimates in equivalent hard-sphere diameters at high density and low temperature, and thus, have generated metastable fluids.

Although in our density functional theory, there is no need to reduce the reference system to an equivalent hard sphere system, we will still adopt the physically reasonable separation of Kang, et al. We now apply these general considerations to the inverse-12 and Lennard-Jones potentials.

IV. B. The Inverse-12 System

The fcc and Bennett structures are reexamined, this time with the interparticle potential having the following form:

$$\phi(r) = \epsilon(\frac{\sigma}{r})^n \qquad \text{(IV.B.1)}$$

where, for our purposes, n=12, σ is the particle diameter, and ϵ is an energy unit. We begin with the fcc lattice.

Using the separation of section IV.A, we evaluate $\beta f_r[\rho(\vec{x})]$ for each reduced temperature $T^*[=k_BT/\epsilon]$ and mean density ρ_o, using $\phi_r(r)$, in the manner of section III, and use $\phi_p(r)$ in the calculation of the meanfield term in equation IV.A.2.

In this way, we were able to obtain coexistence parameters and bulk phase thermodynamic properties for inverse-12 freezing and the solid phase, respectively.

As a result of the form of the potential in IV.B.1, the partition function, and hence thermodynamic properties, of these systems depends not on temperature and density separately, but on a dimensionless parameter, χ:

$$\chi = \rho_o \left(\frac{\epsilon}{k_B T}\right)^{3/n} \sigma^3 \qquad \text{(IV.B.2)}$$

Because of this scaling, the thermodynamic properties and coexistence parameters for these systems in the entire T-ρ plane can be determined from a single isotherm. Specifically, once the values of χ_s and χ_f for a single temperature - density point at melting have been determined, the entire phase diagram may be produced via the relations:

$$\rho_s = \chi_s (T^*)^{3/n}$$

$$\rho_f = \chi_f (T^*)^{3/n} \qquad \text{(IV.B.3)}$$

where the subscripts refer to fluid and solid phases.

The constants χ_s, χ_f have been determined by Hoover et. al. (37) using Monte Carlo calculations. They obtain the following values:

$$\chi_s = 1.193$$

$$\chi_f = 1.141$$

We have used our density functional theory to evaluate the coexistence densities as a function of temperature. The phase diagram thus examined is described by the scaling equations IV.B.3, as expected, with the following values for χ_s, χ_f:

$$\chi_s = 1.2$$

$$\chi_f = 1.165$$

The errors in solid phase and fluid phase densities along the melting line are less than .5 percent and 2 percent, respectively.

Other coexistence parameters calculated by Hoover et. al. are melting entropy and pressure, and the Lindemann ratio. For transition entropy, they find

$$\frac{\Delta S}{NK_B} = .9$$

We obtain the value .96 for this same quantity from equation III.A.4. The Lindemann ratio calculated by them is

$$\theta = .15$$

As in the hard sphere system, we have evaluated the three Lindemann ratios θ_i, θ_T, and θ_m. They are

$$\theta_i = .128$$

$$\theta_T = .07$$

$$\theta_M = .068$$

Comparing the inverse-12 data to that in Table I for the hard sphere potential, we see the effect of compliance on θ and entropy. Temperature increases the number of configurational states available to the system, thus lowering the freezing entropy and raising the Lindemann ratio at melting. It is interesting, though, that at the point of solid mechanical instability, the Lindemann ratios for inverse-12 and hard sphere

systems are very similar. In Figure 5, we show the density dependence of the Lindemann ratio for the inverse-12, fcc system, for the temperature $T^*=2.75$.

As with coexistence densities in equation IV.B.3, the pressure at melting is given as a function of temperature, as a result of scaling, according to the following expression:

$$\beta P_m = C(T^*)^{3/n} \qquad \text{(IV.B.4)}$$

The computer generated value of C is 22.6, while we obtain the value 38.

This discrepancy in melting pressure may not be as bad as it seems, since pressure behavior is notoriously sensitive even to small errors in free energy curves. This understanding explains the excellent values for coexistence densities and freezing entropy, in the face of pressure differences. Undoubtedly, the errors in free energies are due to the lack of liquid correlations in the mean-field term of the free energy. As the density of the solid is increased away from the coexistence region significant errors in the free energy and pressure arise. This occurs because the mean-field contribution to the free energy increases as the fiducial site lattice contracts. The lack of correlation is noticed more at high densities than at low. In order to address thermodynamic properties of the high density solid, above the melting density, we will need to incorporate these correlations in a more realistic manner. This was not a problem with the hard sphere system, where high density behavior was predicted quite accurately. Evidently, in the coexistence region, these correlation errors are not severe.

We now turn our attention to the aperiodic lattice, described in section III.B. When evaluating quantities for this lattice, the separation of the potential is given by equation IV.A.6, with d_{fcc} replaced by d_c, defined in equation III.B.1. With this lattice and potential separation, we have evaluated the systems free energy density, as a function of density, for a series of temperatures, from $T^*=.1$ to $T^*=10$. For all temperatures, the aperiodic solid is metastable, relative to the uniform fluid. In figure 6, we show the degree of metastability versus density for this system, for $T^*=2.75$. As density increases, the metastability increases, as in the hard sphere system. Also shown is the same quantity for the inverse-12, fcc system at the same temperature. The difference in behavior seen between the periodic and aperiodic lattices, for the same interaction potential, indicates the important dependence of thermodynamics on structure. In light of this, future inclusion of fiducial site fluctuations in the aperiodic lattice will presumably change the behavior of the metastability seen in figure 6. It would be most interesting to quantify this change.

We also have evaluated θ_i, the Lindemann ratio at the point of mechanical instability of the solid. This quantity is shown in figure 5, along with the density dependence of the solid phase Lindemann ratio. The temperature is also $T^*=2.75$. When comparing this curve to that shown for the same potential, but with the fcc lattice, it is evident that the Bennett lattice is "tighter" than the fcc lattice at any given density. This fact is manifest in the lower instability density and the lower θ values of the Bennett lattice vis a vis the crystal, at all

densities. This behavior is consistent with the difference in close-packed densities between the two lattice structures, viz. $\rho_{rcp} = 1.216$, $\rho_{ccp} = 1.414$.

Given a specific interaction potential i.e. the inverse-12 potential, we have examined, in figures 5 and 6, the effect of structure on coexistence and thermodynamic properties of these systems. The influence of attractive forces on these same quantities within a specific lattice structure, can be examined via the Lennard-Jones potential, which we study now.

IV.C Lennard-Jonesium

We examine coexistence behavior and thermodynamic properties for the fcc and Bennett (aperiodic) lattices under the influence of the Lennard-Jones (LJ) potential, given by:

$$\phi(r) = 4\varepsilon \left[\left(\frac{\sigma}{r}\right)^{12} - \left(\frac{\sigma}{r}\right)^{6}\right] \qquad \text{(IV.C.1)}$$

where σ is the diameter of the Lennard-Jones particle, and ε is an energy unit.

The difference between IV.C.1 and IV.B.1 lies in the attractive force, which is absent in the inverse-12 potential and present in the Lennard-Jones system, for $r \geq r_m = (2)^{1/6}$. This value represents the position of the potential minimum. The existence of this minimum at finite separation means that, when separating the potential into reference and perturbation parts, according to equation IV.A.6, the value of r^* in IV.A.6 is fixed and equal to r_m, and not temperature dependent, as it is for the inverse-12 potential.

For the fcc lattice, we have obtained coexistence densities for a series of temperatures, and display our results in the LJ phase diagram shown in figure 7. Also displayed are some values obtained from the computer simulation work of Hansen (38) and Hansen and Verlet (39), indicated by crosses.

It is evident from the results that, at high temperatures, agreement is excellent. This is to be anticipated, since, at high temperatures, the attractive potential is negligible relative to the repulsive branch, thus minimizing the error incurred through the use of the mean-field term in the free energy expression, since this term is numerically

small. Also, at high temperatures, the LJ potential, IV.C.1, reduces to the inverse-12 potential, IV.B.1, if we simply redefine the energy scale. Even at $T^*=1.35$, the error in coexistence densities between simulation and our theory does not exceed 5 percent. At lower temperatures, the attractive force becomes more dominant, the mean-field term is numerically more significant, and correlation errors become noticeable. The simulation value for the LJ triple point is $T_t=.7$, while we obtain the value $T_t=.8$.

Although the low temperature phase diagram shows errors, the general feature of the phase diagram is correct. The fractional density change is largest at the triple point and decreases with increasing temperature, tending towards the values obtained for the inverse-12 potential.

For the temperatures $T^*=1.15$, 1.35, 2.74, 5, and 10 melting pressure values from simulation[38] are: 5.68, 9.0, 33, 86, and 231. From our theory, we obtain the following values: 4.4, 6.2, 21.2, 29, and 38. As in the inverse-12 potential system, correlation errors in the fluid free energy are presumably responsible for these differences in melting pressures. In addition, at these high coexistence densities, the Carnahan-Starling virial for the uniform fluid is known to be inaccurate.

Computer simulation at the temperatures $T^*=1.15$, 1.35, and 2.74, for the LJ crystal, gives the following values for the Lindemann ratio: .139, .137, and .149. As with the HS and inverse-12 systems, we have computed the three Lindemann ratios θ_i, θ_T, and θ_m. For the same three temperatures as above, we obtain, for θ_i, the values: .142, .144, and .137. In fact, from $T^*=.8$ to $T^*=10$, we obtain $\theta_i \approx .14$. The average values of θ_T and θ_m averaged over sixteen temperatures, are: $\theta_T \sim .075$,

$\theta_m \sim .068$. In figure 5, we show the density dependence of θ for the LJ, fcc lattice, at the temperature $T^*=10$. At this temperature, θ_i happens to have the value $\theta_i \sim .13$.

For the aperiodic, Bennett lattice, we show the difference in free energy density between uniform fluid and nonuniform solid, versus density, for $T^*=10$, in figure 6. Obviously, the aperiodic solid, in our theory, is metastable for the LJ interaction, as it is for the HS and inverse-12 systems. For all temperatures considered, including values within the range reported by simulation of glassy systems, we obtain the metastable aperiodic solid.

In figure 5, we shown θ versus density for the aperiodic, LJ system at $T^*=10$. The value of θ_i obtained for this system, for all temperatures investigated, is remarkably constant around the value $\theta_i \sim .14$.

When comparing, in figure 5, the stiffness of the LJ crystal and LJ aperiodic solid, we observe the same behavior as that seen in the inverse-12 systems viz. larger fluctuations in the crystal lattice, for a given interaction potential.

V. Discussion and Conclusion

We have developed and presented a new density functional theory which possesses a number of virtues: (1.) simplicity, (2.) remarkable reproduction of HS freezing parameters and high density HS crystalline thermodynamic properties, (3.) a real space description of the nonuniform solid, (4.) the lack of ambiguity concerning the approximation of solid phase correlations with liquid state direct correlation functions, and (5.) the ability to simply extend the analysis to realistic potentials.

We realize, though, that all is not well in Camelot. One must be cautious when dealing with high density and/or low temperature behavior in soft-sphere systems, due to the present lack of correlations in the mean-field contribution to the Helmholtz free energy. We believe it would be profitable to incorporate these correlations in a manner consistent with the spirit of the present theory. Perhaps "optimized" choices of the division into repulsive and attractive forces are possible. Until such time, we must view this theory as a moderate to high temperature [$T^* \geq 1.15$] density functional theory of LJ potential systems for densities in the coexistence region. For the inverse power potentials, the only constraint, at present, is on density: we should limit our investigations to densities in the coexistence region, for general temperatures.

In these temperature and density regimes, our results for the inverse-12 and LJ liquid-crystalline solid transitions show excellent agreement with computer simulation results. For higher densities, the correlation errors become important.

Consequently, if we restrict our view to these regions, we can be confident of our results for the thermodynamics of aperiodic solids, within the limitations of the theory, which are: (1.) we neglect fiducial site fluctuations, which will presumably affect the thermodynamics of the nonuniform solid, in light of the comparisons shown between crystalline and aperiodic solids for the LJ and inverse-12 potentials [Section IV.B and IV.C], and (2.) uncertainty in high density free energy behavior as a consequence of the mean-field approximation.

Within the appropriate temperature and density regions, the affect of an attractive force on the thermodynamics of a repulsive force system may be determined. We have done this by using the correspondence between the inverse-12 potential and the LJ potential at high LJ temperatures [$T^*=10$]. Comparing equations IV.B.1 and IV.C.1, one sees that LJ results for $T^*=10$ correspond to inverse-12 results for $T^*=2.5$. These results are shown in figures 5 and 6. Comparison of data for similar lattice structures allows one to determine the affect of the LJ attractive force on the properties of the repulsive force reference system, for that particular structure.

The computer simulation of Hansen (38) shows that, even at $T^*=10$, where one would expect the influence of the LJ attractive force to be weak, coexistence densities and pressures for the crystal lattice are increased [3.5% for ρ_L, 4.5% for ρ_s], and decreased [22%] respectively, with the inclusion of attractive forces in the lattice. We find similar behavior with our density functional theory. From figure 7 and our inverse-12 results, we find that coexistence densities increase [2% for ρ_L, 2.5% for ρ_s] and melting pressures decrease [24%] when we introduce the attractive force into the crystal lattice, at $T^*=10$. In addition,

figure 5 indicates increased particle fluctuations as the attractive force is included in the lattice for both the aperiodic and crystalline solids.

Computer simulation (38,39) also observes increased mean-squared displacements of particles from fiducial sites when the attractive branch of the LJ potential is included in the system.

One important final point must be made concerning the affect of the attractive force on the properties of repulsive force systems. The Bennett lattice is more closely packed, at a given density, than the fcc lattice, and therefore, should be less affected by attractions than the crystal structure. This is clearly evident in figure 5, where it is observed that particle fluctuations from fiducial sites increase more for the crystalline lattice than for the aperiodic lattice, at the same density and temperature, when incorporating attractive forces into the solid phase.

Now, when one looks at figure 6, one sees that attractive forces have a larger influence on the aperiodic lattice, in terms of free energy differences, than on the crystal lattice. This behavior underscores the need to treat uniform fluid phase correlations more adequately than we have done here, due to the presently demonstrated sensitivity of fluid free energies to attractive perturbations.

Finally, we should mention a limitation in the theory. The direct correlation function derived from our free energy functional yields a structure factor for the uniform fluid which would show a divergence for a sufficiently flexible trial function. For the densities for which we

find a mechanically stable solid, though, our density fluctuations for the solid are incommensurate with those which yield a diverging fluid structure factor.

In future work we intend to treat fluid phase correlations in a consistent and more realistic manner, as well as, to profitably use the simple structure of this theory in the study of various phenomena, among them: freezing in molecular fluids, the liquid-rotator transition, energetics of the Penrose lattice. For HS systems, these problems may be addressed immediately and confidently with our new density functional theory.

Acknowledgements

We thank D. W. Oxtoby for his helpful comments concerning various aspects of the manuscript and theory, especially the caveat of liquid phase instability under flexible trial functions.

Appendix I

In this appendix, we show[40] how equations II.E.1 and II.E.2 are obtained in the small and large α limits, respectively.

Substitution of II.D.1 into II.B.3 gives:

$$\beta F_0' = \left(\frac{\alpha}{\pi}\right)^{3/2} \sum_{i=1}^{N} \int d\bar{x}\, e^{-\alpha(\bar{x}-\bar{R}_i)^2} \left[\frac{3}{2} \ln\left(\frac{\alpha}{\pi}\right) - 1 + \ln\left[\sum_{j=1}^{N} e^{-\alpha(\bar{x}-\bar{R}_j)^2}\right]\right] \qquad \text{(A.I.1)}$$

$$= \sum_{i=1}^{N} \left[\frac{3}{2} \ln\left(\frac{\alpha}{\pi}\right) - 1\right] + \left(\frac{\alpha}{\pi}\right)^{3/2} \sum_{i=1}^{N} \int d\bar{x}\, e^{-\alpha(\bar{x}-\bar{R}_i)^2} \times \ln\left[\sum_{j=1}^{N} e^{-\alpha(\bar{x}-\bar{R}_j)^2}\right] \qquad \text{(A.I.2)}$$

In the large α limit, Gaussian overlap in $\rho(\bar{x})$ is negligible. Therefore, we need consider only nearest-neighbor overlap. Consequently, the second term in equation A.I.2, which we denote T2, becomes:

$$T2 = \left(\frac{\alpha}{\pi}\right)^{3/2} \sum_{i=1}^{N} \int d\bar{x}\, e^{-\alpha(\bar{x}-\bar{R}_i)^2} \ln\left[\sum_{j=1}^{N} e^{-\alpha(\bar{x}-\bar{R}_j)^2}\right]$$

$$= \left(\frac{\alpha}{\pi}\right)^{3/2} \sum_{i \neq j} \int d\bar{x}\, e^{-\alpha(\bar{x}-\bar{R}_i)^2} \ln\left[e^{-\alpha(\bar{x}-\bar{R}_i)^2} + e^{-\alpha(\bar{x}-\bar{R}_j)^2}\right]$$

$$= \left(\frac{\alpha}{\pi}\right)^{3/2} \sum_{i \neq j} \int d\bar{x}\, e^{-\alpha(\bar{x}-\bar{R}_i)^2} \ln\left[e^{-\alpha(\bar{x}-\bar{R}_i)^2} + e^{-\alpha(\bar{x}-\bar{R}_i)^2} e^{-\alpha(\bar{R}_i-\bar{R}_j)^2} \times e^{-2\alpha(\bar{x}-\bar{R}_i)\cdot(\bar{R}_i-\bar{R}_j)}\right]$$

$$= -\frac{3N}{2} + \left(\frac{\alpha}{\pi}\right)^{3/2} \sum_{i \neq j} \int d\bar{x}\, e^{-\alpha(\bar{x}-\bar{R}_i)^2} \ln\left[1 + e^{-\alpha R_{ij}^2} e^{-2\alpha(\bar{x}-\bar{R}_i)\cdot\bar{R}_{ij}}\right] \qquad \text{(A.I.3)}$$

where

$$\vec{R}_{ij} \equiv \vec{R}_i - \vec{R}_j$$

Continuing, we have:

$$T2 = -\frac{3N}{2} + 2\pi\left(\frac{\alpha}{\pi}\right)^{3/2} \sum_{i\neq j} \int_0^\infty x^2 dx\, e^{-\alpha x^2}$$

$$\times \left\{\int_0^1 dy\, \ln\left[1 + e^{-\alpha R_{ij}^2} e^{-2\alpha xyR_{ij}}\right]\right.$$

$$\left. + \int_0^1 dy\, \ln\left[1 + e^{-\alpha R_{ij}^2} e^{2\alpha xyR_{ij}}\right]\right\} \qquad \text{(A.I.4)}$$

Therefore, combining terms A.I.2 and A.I.4, we obtain for the large α limit

$$\beta F_0' = \sum_{i=1}^{N} \left[\frac{3}{2} \ln\left(\frac{\alpha}{\pi}\right) - \frac{5}{2}\right] + 2\pi\left(\frac{\alpha}{\pi}\right)^{3/2} \sum_{i\neq j} \int_0^\infty x^2 dx\, e^{-\alpha x^2}$$

$$\times \int_0^1 dy\, \ln\left\{1 + 2e^{-\alpha R_{ij}^2} \cosh(2\alpha xyR_{ij}) + e^{-2\alpha R_{ij}^2}\right\} \qquad \text{(A.I.5)}$$

$$= \sum_{i=1}^{N} \left[\frac{3}{2} \ln\left(\frac{\alpha}{\pi}\right) - \frac{5}{2}\right] + \pi\left(\frac{\alpha}{\pi}\right)^{3/2} N\rho_o \int d\vec{R}\, g(R)$$

$$\int_0^\infty x^2 dx\, e^{-\alpha x^2} \int_0^1 dy \ln\left\{1 + 2e^{-\alpha R^2} \cosh(2\alpha xyR) + e^{-2\alpha R^2}\right\}$$

$$\qquad \text{(A.I.6)}$$

where, in A.I.6,

$$\vec{R} \equiv \vec{R}_{12} \ .$$

rem A.I.5, one obtains the large-α ideal gas free energy per particle
or a lattice structure described by a set of discrete fiducial site
ectors e.g. the fcc lattice. When the lattice structure is statistical
n nature, one uses equation A.I.6 to obtain $\beta F_o'/N$ in the large-α limit.
pplication of this density functional theory to aperiodic solids would
e an example of a situation in which one would use A.I.6.

In the small-α limit, the overlap of Gaussian peaks in $\rho(\vec{x})$ is
xtensive. To deal with this, we use the Poisson sum formula[41] to re-
ate the real space density peak expansion and the Fourier space density
ve description of $\rho(\vec{x})$, viz:

$$\rho(\vec{x}) = \left(\frac{\alpha}{\pi}\right)^{3/2} \sum_{i=1}^{N} e^{-\alpha(\vec{x}-\vec{x}_i)^2}$$

$$= \sum_{G} \rho_G \, e^{i\vec{G}\cdot\vec{x}}$$

$$= \rho_o + \sum_{G}' \rho_G \, e^{i\vec{G}\cdot\vec{x}} \qquad \text{(A.I.7)}$$

ere Σ' means $\vec{G} \neq 0$ in A.I.7. In A.I.7 ρ_o is the infinite-wavelength
ane wave state, and can be identified with the mean density of the
stem. The coefficients in equation A.I.7 are given by

$$\rho_G = \frac{1}{V} \sum_{i=1}^{N} e^{-i\vec{G}\cdot\vec{x}_i} \, e^{-G^2/4\alpha} \qquad \text{(A.I.8)}$$

ere V is the systems volume. Substitution of A.I.7 into II.B.3
elds:

$$\beta F_0' = \int d\vec{x} \, [\rho_o + \sum_{G}' \rho_G \, e^{i\vec{G}\cdot\vec{x}}][\ln(\rho_o) - 1$$

$$+ \ln[1 + \frac{1}{\rho_o} \sum_{G}' \rho_G \, e^{i\vec{G}\cdot\vec{x}}]] \qquad \text{(A.I.9)}$$

We write $\beta F_0'$ in Fourier space, as in equation A.I.9, so that one may use the orthogonality property of the density waves, to simplify the evaluation of the ideal gas free energy. Since the density distribution, $\rho(\overline{x})$, in the small-α limit is very flat, a plane wave representation of $\rho(\overline{x})$, offered by a low order Fourier expansion, is appropriate.

Using the expansion of the logarithm, and noting that

$$\sum_{G}' \rho_G \, \delta(G) = 0$$

where $\delta(G)$ is the Dirac delta function, we have, after some manipulations,

$$\beta F_0' = N[\ln(\rho_o) - 1] + \rho_o \int d\overline{x} \left[-\frac{1}{2\rho_o^2} \sum_{G_1} \sum_{G_2} \rho_{G_1} \rho_{G_2} e^{i\overline{x}\cdot(\overline{G}_1+\overline{G}_2)} + \ldots \right] + \int d\overline{x} \left[\frac{1}{\rho_o} \sum_{G_1} \sum_{G_2} \rho_{G_1} \rho_{G_2} e^{i\overline{x}\cdot(\overline{G}_1+\overline{G}_2)} - \ldots \right] \qquad \text{(A.I.10)}$$

In A.I.10, we have ignored terms that involve sums over three or more reciprocal space vectors, due to the plane wave nature of $\rho(\overline{x})$ in the small-α limit. We write A.I.10 as

$$\beta F_0' = N[\ln(\rho_o)-1] + T3 \qquad \text{(A.I.11)}$$

where

$$T3 = \frac{V}{2\rho_o} \sum_{G}' |\rho_G|^2 \qquad \text{(A.I.12)}$$

Expression A.I.12 is obtained with the use of the integral representation of the delta function. Substitution of A.I.8 into A.I.12 yields

$$T3 = \frac{1}{2\rho_o V} \sum_{G}{}' \sum_{i=1}^{N} \sum_{j=1}^{N} e^{-G^2/2\alpha} e^{-i\vec{G}\cdot(\vec{R}_i - \vec{R}_j)} \qquad \text{(A.I.13)}$$

We now rewrite the restricted sum in A.I.13 in terms of the unrestricted sum and the zero wavevector component, i.e.

$$T3 = \frac{1}{2\rho_o} \sum_{i=1}^{N} \sum_{j=1}^{N} \frac{2\pi}{(2\pi)^3} \int_0^\infty G^2 dG\, e^{-G^2/2\alpha}$$

$$\int_{-1}^{1} dy\, e^{-iGyR_{ij}} - \frac{\rho_o V}{2} \qquad \text{(A.I.14)}$$

In A.I.14, we have expressed the unrestricted sum in terms of an integral, in the limit of infinite system size. Performing the simple Gaussian integrals, and writing the double sum as a self-term (i=j) and a distinct term (i≠j), we finally obtain:

$$T3 = \frac{1}{4\sqrt{2}} \left(\frac{\alpha}{\pi}\right)^{3/2} \frac{N}{\rho_o} + \frac{1}{4\sqrt{2}} \left(\frac{\alpha}{\pi}\right)^{3/2} \left(\frac{1}{\rho_o}\right) \sum_{i \neq j} e^{-\alpha R_{ij}^2/2} - \frac{\rho_o V}{2} \qquad \text{(A.I.15)}$$

where the distinct term involves a sum over a lattice described by a set of discrete fiducial sites, as in equation A.I.5. For a statistical lattice, we express A.I.15 in terms of a statistical distribution of fiducial sites in the system:

$$T3 = \frac{1}{4\sqrt{2}} \left(\frac{\alpha}{\pi}\right)^{3/2} \frac{N}{\rho_o} + \frac{N}{4\sqrt{2}} \left(\frac{\alpha}{\pi}\right)^{3/2} \int d\vec{R}\, g(R) e^{-\frac{\alpha}{2} R^2} - \frac{\rho_o V}{2} \qquad \text{(A.I.16)}$$

where $\vec{R}$ in A.I.16 was given before in A.I.6.

Combining A.I.11 and A.I.16 gives the small-α limit to the ideal gas free energy per particle.

Appendix II:

We start by substituting II.D.1 into II.C.9. The result is:

$$\eta(\alpha) = -\frac{1}{8N}\sum_{i,j}\left(\frac{\alpha}{\pi}\right)^3 \int d\bar{r}\, d\bar{r}'\, f(|\bar{r}-\bar{r}'|)\, e^{-\alpha(\bar{r}-\bar{r}_i)^2}\, e^{-\alpha(\bar{r}'-\bar{r}_j)^2} \tag{A.II.1}$$

The summation in A.II.1 is over all values of i and j. We therefore can separate $\eta(\alpha)$ into a self-term, with i=j, and a lattice term, i≠j. The self term will obviously be independent of the fiducial site lattice, while the lattice term will depend on the assumed lattice structure. Therefore, we write:

$$\eta(\alpha) = \eta_s(\alpha) + \eta_\ell(\alpha) \tag{A.II.2}$$

For the self term, we have:

$$\eta_s(\alpha) = -\frac{1}{8N}\sum_{i=1}^{N}\left(\frac{\alpha}{\pi}\right)^3 \int d\bar{r}d\bar{r}'\, f(|\bar{r}-\bar{r}'|)\, e^{-\alpha(\bar{r}-\bar{r}_i)^2} e^{-\alpha(\bar{r}'-\bar{r}_i)^2} \tag{A.II.3}$$

Without loss of generality, we may set all $\bar{r}_i$ to zero. Therefore, A.II.3 becomes:

$$\eta_s(\alpha) = -\frac{N}{8N}\left(\frac{\alpha}{\pi}\right)^3 \int d\bar{r}d\bar{r}'\, f(|\bar{r}-\bar{r}'|)\, e^{\alpha r^2}\, e^{-\alpha(r')^2} \tag{A.II.4}$$

Letting $\bar{x} = \bar{r} - \bar{r}'$, substituting in A.II.4, and performing some simple Gaussian integrals gives:

$$\eta_s(\alpha) = -\frac{1}{8}\left(\frac{\alpha}{2\pi}\right)^{3/2} \int d\bar{x}\, f(x)\, e^{-\alpha x^2/2} \tag{A.II.5}$$

Equation A.II.5 is the working equation for $\eta_s(\alpha)$. Given any arbitrary repulsive potential, $\phi(x)$, one may trivially evaluate $\eta_s(\alpha)$ for each α value. Continuing with the lattice term, we have:

$$\eta_2(\alpha) = -\frac{1}{8N} \sum_{i \neq j} \left(\frac{\alpha}{\pi}\right)^3 \int d\bar{r}\, d\bar{r}'\, f(|\bar{r} - \bar{r}'|)$$

$$e^{-\alpha(\bar{r}-\bar{r}_i)^2}\, e^{-\alpha(\bar{r}'-\bar{r}_j)^2} \qquad \text{(A.II.6)}$$

Defining $\bar{R} = \bar{r}_i - \bar{r}_j$, and setting $\bar{r}_i$ to zero, as in $\eta_3(\alpha)$, one obtains

$$\eta_2(\alpha) = -\frac{1}{8} \sum_{R} \left(\frac{\alpha}{\pi}\right)^3 \int d\bar{r} d\bar{r}'\, f(|\bar{r} - \bar{r}'|) e^{-\alpha r^2}\, e^{-\alpha(\bar{r}'+\bar{R})^2} \qquad \text{(A.II.7)}$$

Letting $\bar{x} = \bar{r} - \bar{r}'$, substituting in A.II.7, and evaluating some Gaussian integrals yields a working expression for $\eta_2(\alpha)$:

$$\eta_2(\alpha) = -\frac{\pi\rho_o}{2} \left(\frac{\alpha}{2\pi}\right)^{1/2} \int_0^\infty r\,dr\, g(r) \int_0^\lambda x\,dx\, f(x) \left\{ e^{-\frac{\alpha}{2}(r-x)^2} - e^{-\frac{\alpha}{2}(r+x)^2} \right\} \qquad \text{(A.II.8)}$$

In A.II.8, $\rho_o g(r)$ is the probability distribution of fiducial sites. For the disordered solid, it is given by Bennett (32). For the fcc crystal, it is a sum of delta functions, centered at each lattice site. In this case, A.II.8 transforms to:

$$\eta_2(\alpha) = -\frac{1}{8} \left(\frac{\alpha}{2\pi}\right)^{1/2} \sum_{R} \left(\frac{1}{R}\right) \int_0^\lambda x\,dx\, f(x) \left\{ e^{-\frac{\alpha}{2}(R-x)^2} - e^{-\frac{\alpha}{2}(R+x)^2} \right\} \qquad \text{(A.II.9)}$$

where $\bar{R}$ is a Bravais lattice vector in the fcc crystal.

With these expressions for $\eta_3(\alpha)$ and $\eta_2(\alpha)$, one can easily evaluate II.C.9, for any repulsive potential and any fiducial site distribution, and thus implement this convenient density functional theory.

Appendix III

We would like to demonstrate that, in the limit of close-packing, the pressure of the solid phase behaves like that of free volume theory i.e. equation III.A.8. We start with the α-dependent free energy, given by

$$\beta f(\alpha) = \frac{3}{2} \ln \left(\frac{\alpha}{\pi}\right) - \frac{5}{2} + \frac{\eta(\alpha)[4-3\eta(\alpha)]}{[1-\eta(\alpha)]^2} \qquad \text{(A.III.1)}$$

In order to find pressure, one needs the density-dependent free energy. Thus, one needs to find $\alpha_{min}(\rho_o)$, where α_{min} is found from minimization of A.III.1.

Minimization of A.III.1 gives the following:

$$0 = \frac{3}{2\alpha} + \frac{[4-2\eta(\alpha)]}{[1-\eta(\alpha)]^3} \frac{\partial \eta(\alpha)}{\partial \alpha} \qquad \text{(A.III.2)}$$

From A.II.2, differentiation of $\eta(\alpha)$ implies differentiation of lattice and self terms. Proceeding, we have, from A.II.5, the following:

$$\frac{\partial \eta_s(\alpha)}{\partial \alpha} = \frac{-3\sqrt{\alpha}}{16(2\pi)^{3/2}} \int d\bar{x}\, f(x)\, e^{-\alpha x^2/2}$$

$$+ \left(\frac{1}{16}\right)\left(\frac{\alpha}{2\pi}\right)^{3/2} \int x^2 d\bar{x}\, f(x)\, e^{-\alpha x^2/2} \qquad \text{(A.III.3)}$$

For the hard-sphere system, evaluation of the integrals in A.III.3 and cancellation of terms results in:

$$\frac{\partial \eta_s(\alpha)}{\partial \alpha} = \left(\frac{1}{8}\right)\left(\frac{\alpha}{2\pi}\right)^{1/2} e^{-\alpha\sigma^2/2} \qquad \text{(A.III.4)}$$

where σ is the hard-sphere diameter. For the lattice term, we need sum only over nearest-neighbors, since for large α, overlap of Gaussians is negligible. Therefore, from A.II.9, we obtain:

$$\eta_\ell(\alpha) = -\left(\frac{1}{8}\right)\left(\frac{\alpha}{2\pi}\right)^{1/2} \left(\frac{z}{d}\right) \int_0^\sigma x\,dx\, f(x)\left[e^{-\frac{\alpha}{2}(d-x)^2} - e^{-\frac{\alpha}{2}(d+x)^2}\right]$$

(A.III.5)

where z is the number of nearest-neighbors, and d is the nearest-neighbor fiducial site separation. Differentiation of A.III.5, and retention of the maximum term gives:

$$\frac{\partial \eta_\ell(\alpha)}{\partial \alpha} = -\left(\frac{z}{16d}\right)\left(\frac{\alpha}{2\pi}\right)^{1/2} \int_{\lambda_1}^{\lambda_2} y^2 dy(d-y)e^{-\alpha y^2/2} \qquad \text{(A.III.6)}$$

where $\lambda_1 = d-\sigma$, $\lambda_2 = d$, and $y = d-x$. Evaluation of A.III.6, in terms of error functions and exponentials, gives, in the limit of large α, the following expression for $\eta_\ell'(\alpha)$:

$$\eta_\ell'(\alpha) \simeq -\frac{z\,(d-\sigma)}{16\,(2\pi\alpha)^{1/2}}\, e^{-\alpha(d-\sigma)^2/2} \qquad \text{(A.III.7)}$$

In the large α limit, $\eta(\alpha)$ reduces to the following expression:

$$\eta(\alpha) \sim \frac{1}{8} + \frac{z}{16}\left\{1-\mathrm{erf}\left[\sqrt{\frac{\alpha}{2}}(d-\sigma)\right]\right\} \qquad \text{(A.III.8)}$$

where $\sqrt{\frac{\alpha}{2}}\,(d-\sigma) \to$ constant $(\simeq .9)$ as $\alpha \to \infty$.

Therefore, from A.II.2, A.III.4, A.III.7, and A.III.8, A.III.2 becomes:

$$0 = \frac{3}{2\alpha} + C_1\left[\frac{1}{8}\left(\frac{\alpha}{2\pi}\right)^{1/2} e^{-\alpha_0^2/2} - \frac{z}{16}\frac{(d-\sigma)}{(2\pi\alpha)^{1/2}}\, e^{-\alpha(d-\sigma)^2/2}\right] \qquad \text{(A.III.9)}$$

where C_1 is some constant.

Rearranging A.III.9 gives:

$$D = \sqrt{\alpha}\,(d-\sigma)\, e^{-\alpha(d-\sigma)^2/2} \qquad \text{(A.III.10)}$$

where D is a constant. Graphical solution of A.III.10 yields the following expression for α_{min}:

$$\alpha_{min} = \frac{c^2}{(d-\sigma)^2} \qquad \text{(A.III.11)}$$

where $c^2 \simeq 1.67$

In general,

$$d \sim \frac{1}{(\rho_o)^{1/3}} \qquad \text{(A.III.12)}$$

For the fcc crystal, III.A.7 obtains. For the Bennett lattice, we use III.B.1. Substitution of A.III.12 into A.III.11 gives the density dependent equilibrium α value in the high density limit:

$$\alpha_{min}(\rho_o) = \frac{E^2}{[(\rho_o)^{-1/3} - (\rho_{cp})^{1/3}]^2} \qquad \text{(A.III.13)}$$

where ρ_{cp} designates the close-packed state and $E^2 \simeq 1.32$. Substitution of A.III.13 into A.III.1, and neglecting the interaction terms at these high densities gives the following free energy behavior:

$$\beta f(\rho_o) = \ell n(\rho_o) - 3\ell n[1 - (\frac{\rho_o}{\rho_{cp}})^{1/3}] + \text{constants} \qquad \text{(A.III.14)}$$

Expansion of the argument in the second term of equation A.III.14 to second order about the close-packed state, and further expansion of the logarithm of the quadratic term, yields the following pressure behavior, after appropriate differentiation:

$$\frac{\beta P}{\rho_o^2} = \frac{\partial(\beta f)}{\partial \rho_o} = \frac{1}{\rho_o} + \frac{1}{\rho_{cp}} + \frac{3}{(\rho_{cp} - \rho_o)} \qquad \text{(A.III.15)}$$

Alder, et. al. (31) write the high density virial in the following form:

$$\frac{\beta P}{\rho_o} = \frac{3\rho_o}{(\rho_{cp} - \rho_o)} + C_o + \ldots \qquad \text{(A.III.16)}$$

where the higher order virial terms vanish as the close-packed state is approached. Comparison of A.III.16 and A.III.15 shows that our theory

predicts the value of C_o to be 2. "Exact" simulation results determine C_o to be 2.56. The value of C_o which we obtain is also that given by self-consistent free volume theory. In addition, equations A.III.15 and A.III.16 indicate that our free energy density functional provides the proper pressure behavior, that of III.A.8.

References

1. Y. Singh, J. P. Stoessel, and P. G. Wolynes, Phys. Rev. Lett., 54, 1059 (1985).
2. M. Baus and J. L. Colot, Mol. Phys. (in press).
3. A. D. J. Haymet (preprint).
4. L. Onsager, Ann. N.Y. Acad. Sci., 51, 627 (1949).
5. J. G. Kirkwood and E. Monroe, J. Chem. Phys., 8, 845 (1940); 9, 514 (1941).
6. B. J. Alder and T. E. Wainwright, J. Chem. Phys., 27, 1208 (1957).
7. M. S. Wertheim, Phys. Rev. Lett., 10, 321 (1963); J. Math. Phys., 5, 643 (1964).
8. H. C. Longuet-Higgins and B. Widom, Mol. Phys., 8, 549 (1964).
9. L. Verlet, Phys. Rev. 163, 201 (1968).
10. See, for example, J. P. Hansen and I. R. McDonald in Theory of Simple Liquids (Academic Press, N.Y.; 1976).
11. T. V. Ramakrishnan and M. Yussouff, Phys. Rev. B, 19, 2775 (1979).
12. A. D. J. Haymet and D. W. Oxtoby, J. Chem. Phys., 74, 2559 (1981); D. W. Oxtoby and A. D. J. Haymet, J. Chem. Phys., 76, 6262 (1982).
13. M. D. Lipkin and D. W. Oxtoby, J. Chem. Phys., 79, 1939 (1983).
14. Y. Singh, Phys. Rev. A30, 583 (1984).
15. P. Harrowell and D. W. Oxtoby, J. Chem. Phys., 80, 1639 (1984).
16. A. D. J. Haymet, J. Chem. Phys., 78, 4641 (1983).
17. P. Tarazona, Mol. Phys., 52, 81 (1984).
18. M. Baus and J. L. Colot, J. Phys. C. (in press).
19. Gerald L. Jones and Udayan Mohanty, Mol. Phys. (in press).
20. P. Tarazona, Phys. Rev. A, 31, 2672 (1985).
21. D. Frenkel and J. P. McTague, Ann. Rev. Phys. Chem., 31, 491 (1980).
22. David Young and B. J. Alder, J. Chem. Phys., 60, 1254 (1974).
23. Z. W. Salsburg and W. W. Wood, J. Chem. Phys., 42, 3852 (1965).
24. A. J. M. Yang, P.D. Fleming, and J. H. Gibbs, J. Chem. Phys., 64, 3732 (1976).

25. T. Morita and K. Hiroike, Prog. Theor. Phys., 25, 537 (1961).

26. N. F. Carnahan and K. E. Starling, J. Chem. Phys., 51, 635 (1969).

27. F. H. Ree and W. G. Hoover, J. Chem. Phys., 40, 939 (1964); 46, 4181 (1967).

28. F. A. Lindemann, Z. Physik., 11, 609 (1910).

29. W. G. Hoover and F. H. Ree, J. Chem. Phys., 49, 3609 (1968).

30. D. Henderson and E. W. Grundke, J. Chem. Phys., 63, 601 (1975).

31. B. J. Alder, W. G. Hoover, and D. A. Young, J. Chem. Phys., 49, 3688 (1968).

32. C. H. Bennett, J. Appl. Phys., 43, 2727 (1972).

33. J. D. Bernal, Proc. Roy. Soc. London, Ser. A. 280, 299 (1964).

34. L. V. Woodcock and C. A. Angell, Phys. Rev. Lett., 47, 1129 (1981).

35. H. S. Kang, C. S. Lee, T. Ree and F. H. Ree, J. Chem. Phys., 82, 414 (1985).

36. H.C. Andersen, J. D. Weeks, and D. Chandler, Phys. Rev. A4, 1597 (1971).

37. W. G. Hoover, M. Ross, K. W. Johnson, D. Henderson, J. A. Barker, and B. C. Brown, J. Chem. Phys., 52, 4931 (1970).

38. J. P. Hansen, Phys. Rev. A, 2, 221 (1970).

39. J. P. Hansen and L. Verlet, Phys. Rev. 184, 151 (1969).

40. Y. Singh, unpublished notes.

41. P. M. Morse and H. Feshbach, Methods of Theoretical Physics (McGraw Hill, 1953) Chap. 4.

42. A. D. J. Haymet and D. W. Oxtoby, J. Chem. Phys. (submitted).

43. J. P. Stoessel and P. G. Wolynes, J. Chem. Phys., 80, 4502 (1984).

44. B. Bagchi, C. Cerjan, and S. A. Rice, J. Chem. Phys., 79, 5595 (1983); 6222 (1983); B. Bagchi, C. Cerjan, U. Mohanty, and S. A. Rice, Phys. Rev. B, 29, 2857 (1984); M. Baus, Mol. Phys. 50, 543 (1983); 51, 211 (1984).

45. Subir Sachdev and D. R. Nelson (preprint).

Table I. Coexistence parameters for the HS freezing transition from various theories and computer simulation

Source (ref)	ρ_f	ρ_s	$(\rho_s-\rho_f)/\rho_f$ %	βP_m	$\Delta S/Nk_B$	θ_i	θ_T	θ_m
A(29)	.939-.948	1.036-1.045	.103	11.7	1.16	--	--	.126
B (This work)	.96	1.07	.114	13.	1.3	.125	.068	.053
C(19)	.9461	1.0525	.112	---	---	--	--	.048
D(17)	.8917	.9662	.084	---	---	--	--	.084
E(17)	1.0635	1.1903	.119	---	---	--	--	--
F(20)	.9433	1.061	.125	---	---	--	--	--
G(2)	.993	1.083	.091	12.3(v) 16.1(c)	1.03(v) 1.36(c)	.149	.088	.074
H(16)	.976	1.035	.06	---	---	--	--	.05
I(42)	.946	1.03	.089	11.6	1.0	--	--	--

ρ_f = fluid phase coexistence density

ρ_c = solid phase coexistence density

βP_m = melting pressure

$\Delta S/Nk$ = entropy change at melting

θ_i = Lindemann ratio at mechanical instability

θ_T = Lindemann ratio at marginal thermodynamic stability

θ_m = Lindemann ratio at coexistence

c(v) = use of compressibility (virial) PY equation of state.

Figure Captions

Figure 1: For $\rho_o^* = 1.0$, the ideal gas Helmholtz free energy per particle (solid line), the interaction Helmholtz free energy per particle (dotted line), and the total Helmholtz free energy per particle (dashed line), versus α.

Figure 2: HS free energy density, versus density, for the following structures: uniform fluid (solid curve), fcc crystal (dotted curve), and Bennett lattice (dashed curve).

Figure 3: HS compressibility ($\beta P/\rho_o$), versus ρ_o. We show the Salsburg-Wood pressure, equation III.A.8, with $\rho_{cp} = 1.216$ (solid curve) the high density pressure in the Bennett lattice (dashed curve), and both the high density crystal pressure along with equation III.A.8, with $\rho_{cp} = \sqrt{2}$ (dotted curve).
Note: the dotted curve is actually <u>both</u> curves superimposed.

Figure 4: HS Lindemann ratio versus ρ_o for: crystal (dotted curve) and Bennett lattice (dashed curve).

Figure 5: Soft-sphere Lindemann ratio versus ρ_o for: inverse-12 potential and Bennett lattice (dashed curve), the LJ potential and Bennett lattice (solid curve), the inverse-12 crystal (dotted curve), and the LJ crystal (dashed-dotted).

Figure 6: Free energy density difference, relative to the uniform fluid, versus ρ_o, for the following systems: inverse-12 potential and Bennett lattice (dashed curve), LJ potential and Bennett lattice (solid curve), the LJ crystal (dashed-dotted), and the inverse-12 crystal (dotted).

Figure 7: Phase diagram (solid curves) for the liquid-crystalline solid phase transition in the LJ system. Also shown (crosses) are values obtained from computer simulation.

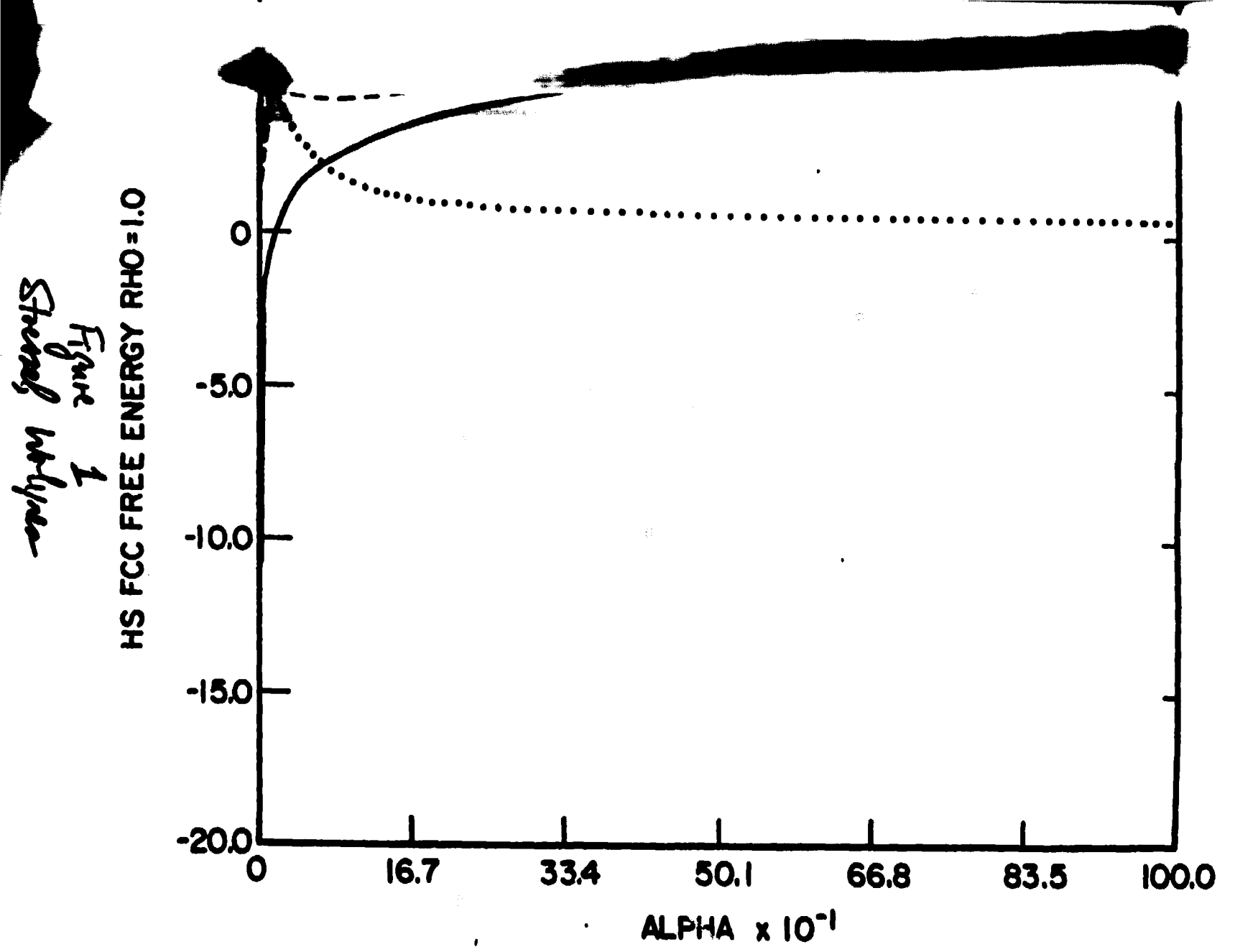

Figure 1
Stewart Murphy

Figure 2
Strenski Whitmer

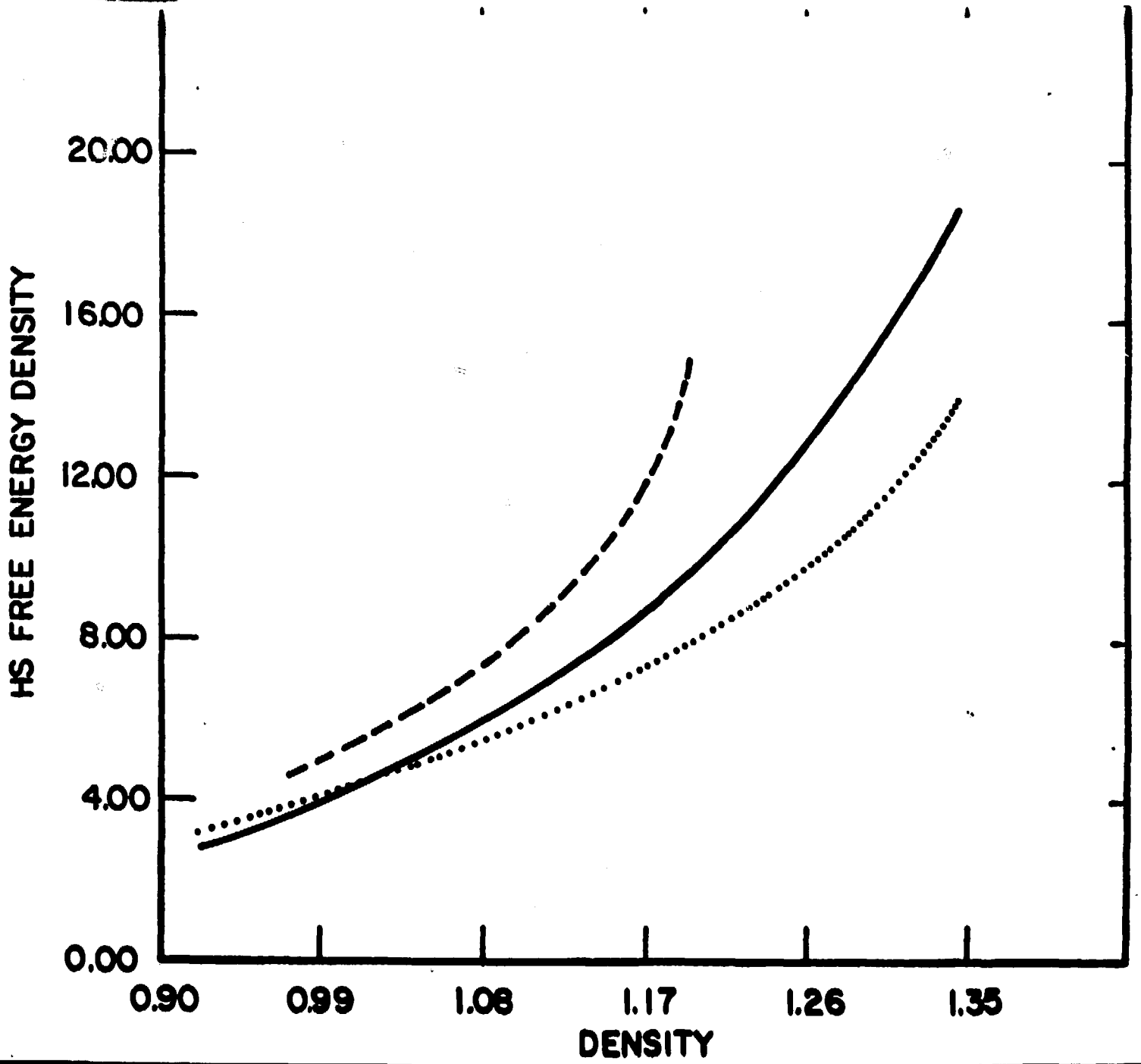

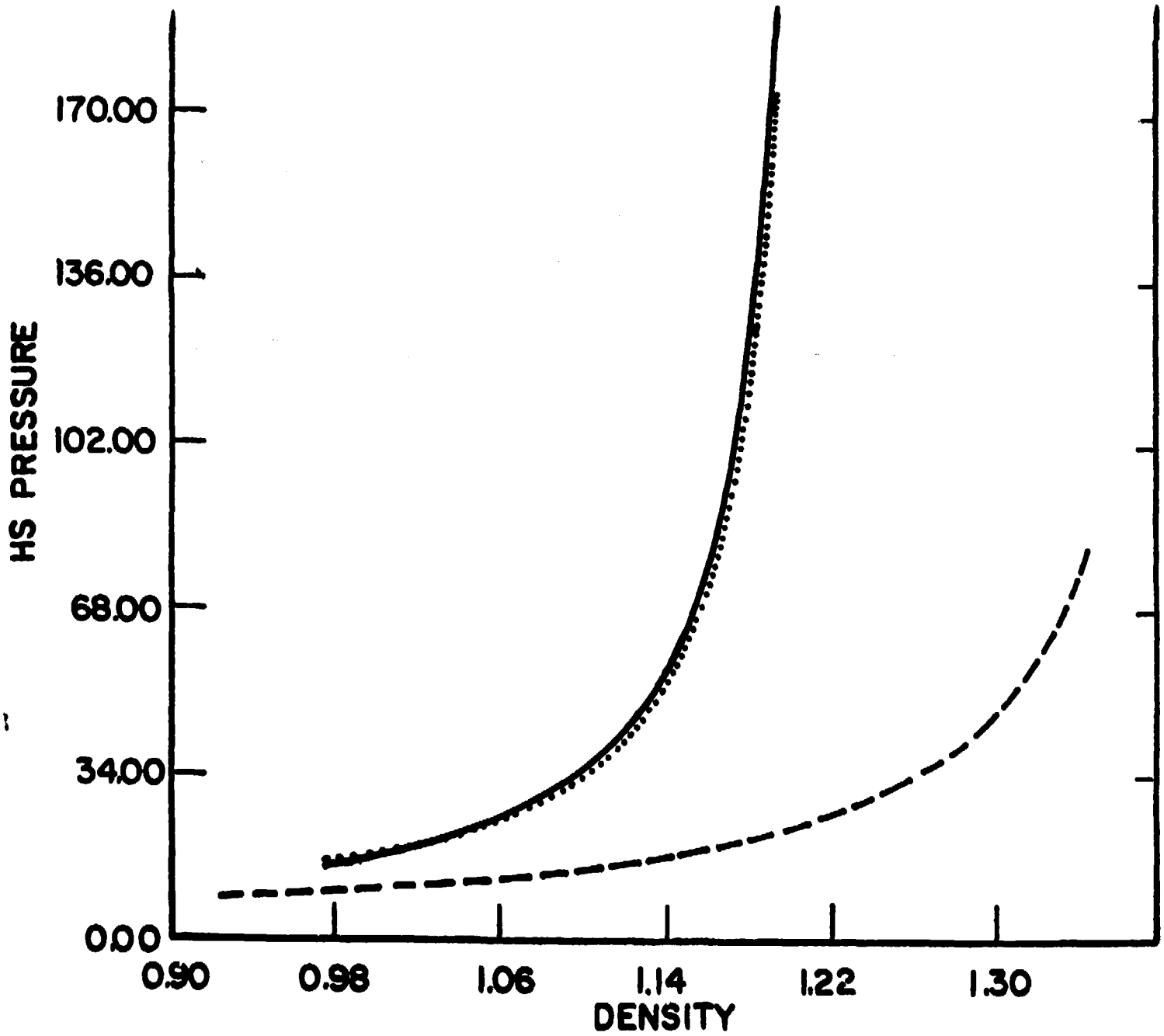

Figure 3
Strand Wahyman

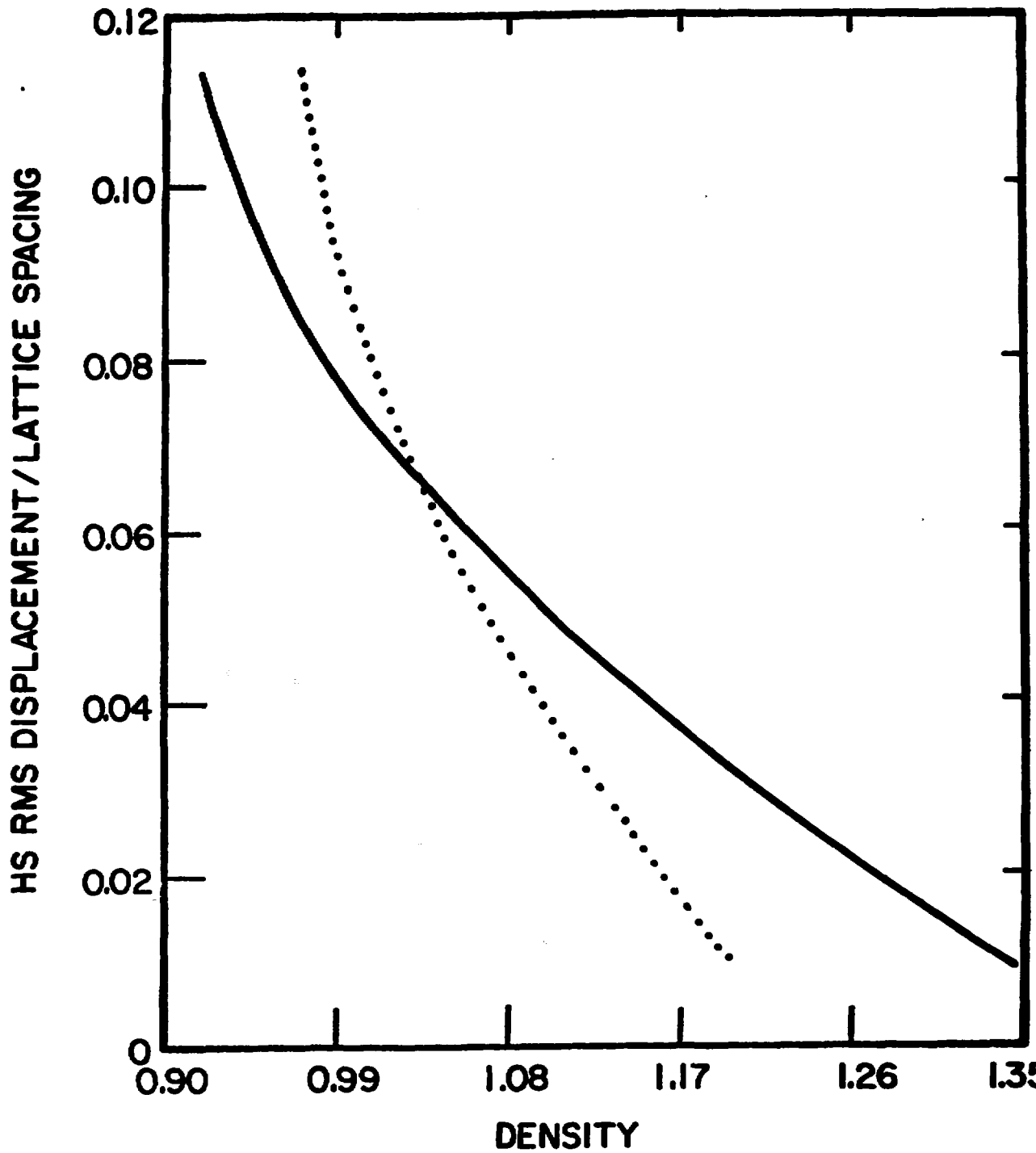

Figure 4
Stossel, Wolynes

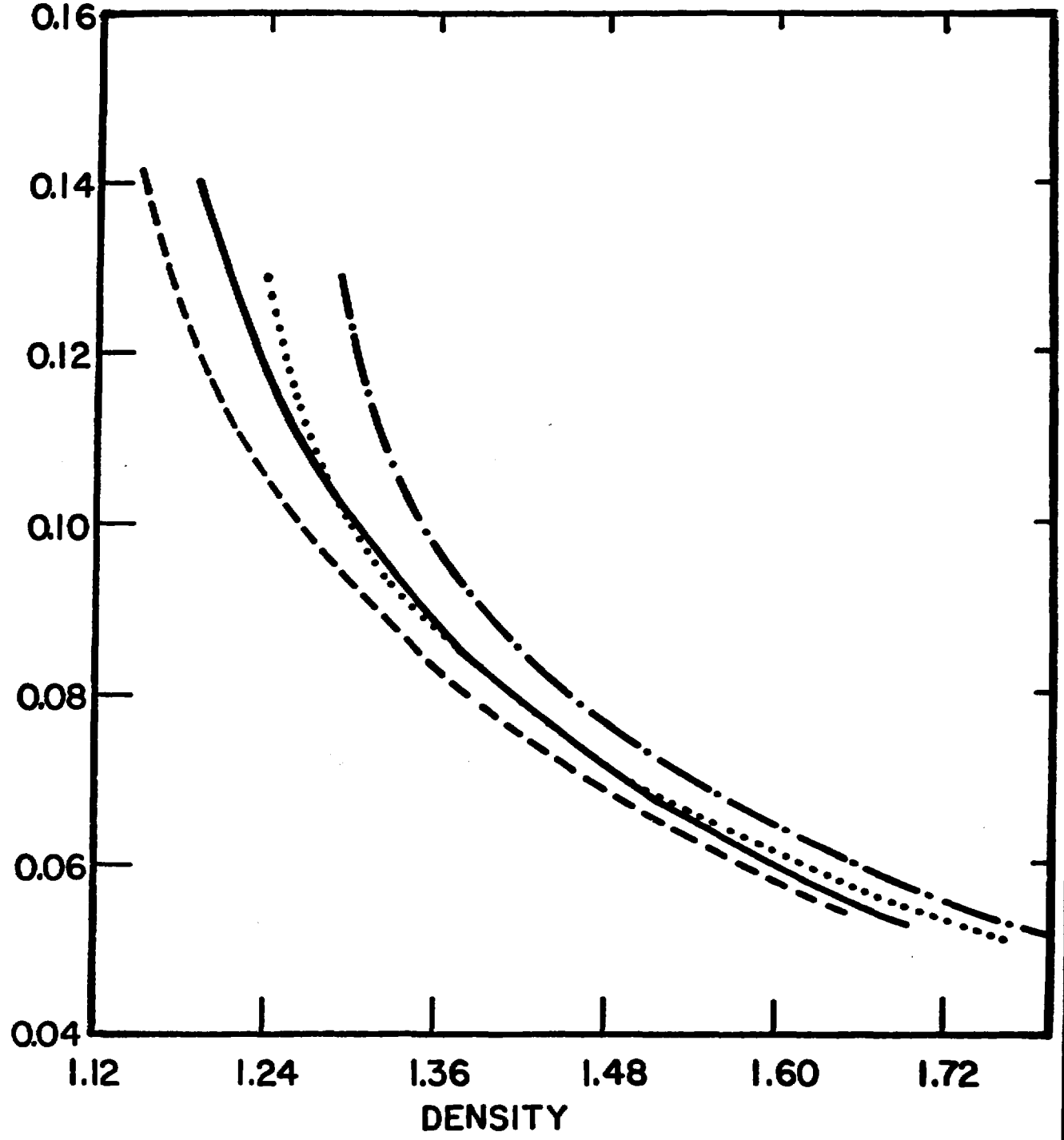

Figure 5
Stoessel, Wolynes

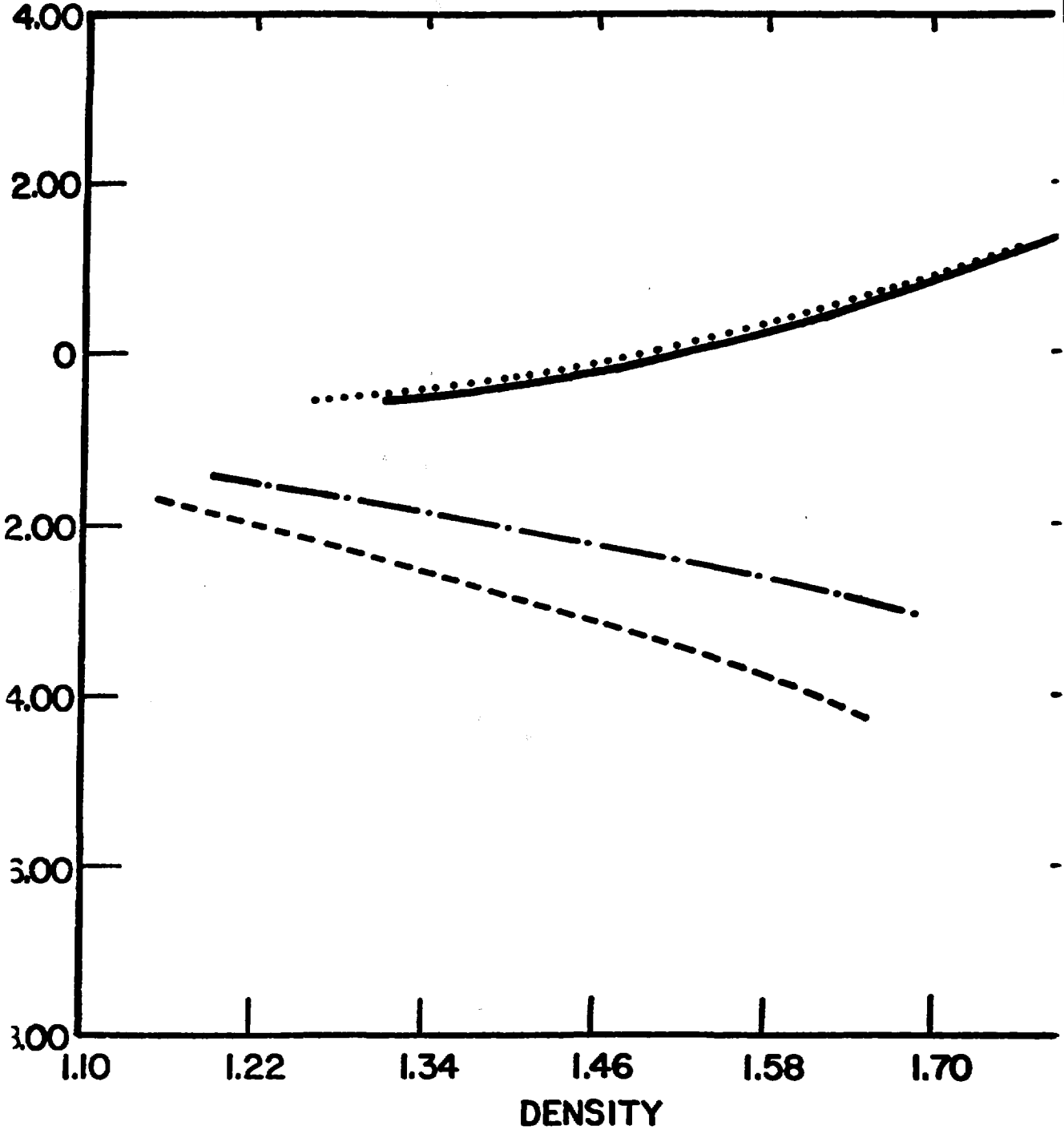

Figure 6
Stoessel, Wolynes

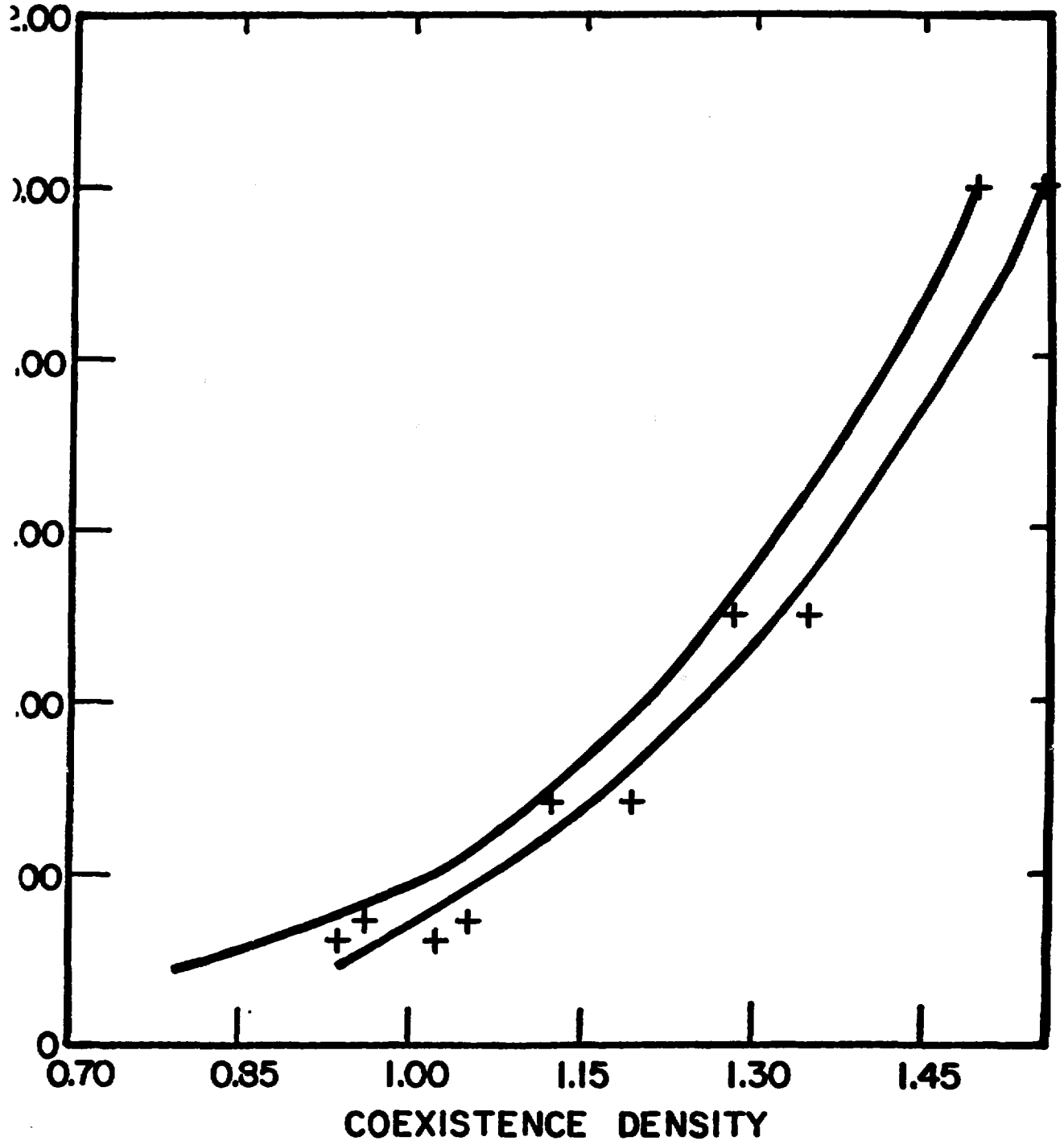

Figure 7

Stoessel, Wolynes